IRANIAN JOURNAL OF SCIENCE AND TECHNOLOGY: TRANSACTIONS OF MECHANICAL ENGINEERING

ISSN: 2228-6187 (print version); ISSN: 2364-1835 (electronic version)
Publisher: Springer; Impact factor = 0.732; Accepted July 13, 2018

SLIP AND HALL CURRENT EFFECTS ON JEFFREY FLUID SUSPENSION FLOW IN A PERISTALTIC HYDROMAGNETIC BLOOD MICROPUMP

K. Ramesh[a], D. Tripathi[b,*], O. Anwar Bég[c] and A. Kadir[d]

[a]*Department of Mathematics, Lovely Professional University, Jalandhar, Punjab, 144411, India*
[b]*Department of Mechanical Engineering, Manipal University Jaipur, Rajasthan, 303007, India*
[c]*Fluid Mechanics and Propulsion, Aeronautical and Mechanical Engineering, University of Salford, Newton Building, G77, The Crescent, Salford, M54WT, England, UK.*
[d]*Materials, Corrosion and Structures, Aeronautical and Mechanical Engineering, University of Salford, Newton Building, G79, The Crescent, Salford, M54WT, England, UK.*
**Corresponding author- email: dharmendra.tripathi@jaipur.manipal.edu*

ABSTRACT

The magnetic properties of blood allow it to be manipulated with an electromagnetic field. Electromagnetic blood flow pumps are a robust technology which provide more elegant and sustainable performance compared with conventional medical pumps. Blood is a complex multi-phase suspension with non-Newtonian characteristics which are significant in micro-scale transport. Motivated by such applications, in the present article a mathematical model is developed for magnetohydrodynamic (MHD) pumping of blood in a deformable channel with peristaltic waves. A Jeffery's viscoelastic formulation is employed for the rheology of blood. A two-phase fluid-particle ("dusty") model is utilized to better simulate suspension characteristics (plasma and erythrocytes). Hall current and wall slip effects are incorporated to achieve more realistic representation of actual systems. A two-dimensional asymmetric channel with dissimilar peristaltic wave trains propagating along the walls is considered. The governing conservation equations for mass, fluid and particle momentum are formulated with appropriate boundary conditions. The model is simplified using of long wavelength and creeping flow approximations. The model is also transformed from the fixed frame to the wave frame and rendered non-dimensional. Analytical solutions are derived. The resulting boundary value problem is solved analytically and exact expressions are derived for the fluid velocity, particulate velocity, fluid/particle fluid and particulate volumetric flow rates, axial pressure gradient, pressure rise and skin friction distributions are evaluated in detail. Increasing Hall current parameter *reduces* bolus growth in the channel, particle phase velocity and pressure difference in the augmented pumping region whereas it *increases* fluid phase velocity, axial pressure gradient and pressure difference in the pumping region. Increasing the hydrodynamic slip parameter accelerates both particulate and fluid phase flow at and close to the channel walls, enhances wall skin friction, boosts pressure difference in the augmented pumping region and increases bolus magnitudes. Increasing viscoelastic parameter (stress relaxation time to retardation time ratio) decelerates the fluid phase flow, accelerates the particle phase flow, decreases axial pressure gradient, elevates pressure difference in the augmented pumping region and reduces pressure difference in the pumping region. Increasing drag particulate suspension parameter decelerates the particle phase velocity, accelerates the fluid phase velocity, strongly elevates axial pressure gradient and reduces pressure difference (across one wavelength) in the augmented pumping region. Increasing particulate volume fraction density enhances bolus magnitudes in both the upper and lower zones of the channel and elevates pressure rise in the augmented pumping region.

KEYWORDS: *Peristaltic propulsion;Magnetohydrodynamics; Particle-fluid suspension; Viscoelasticity; Hall current; Slip boundary conditions; Electromagnetic biomimetic blood pumps*.

NOMENCLATURE

Roman

a_1, a_2 : Wave amplitudes

a : Amplitude ratio of the upper wall wave

b : Amplitude ratio of the lower wall wave

B_0 : Magnetic field

c : Wave speed

e : Charge of ions

F : Dimensionless time-mean flow in the wave frame

h_1, h_2 : Dimensionless wall deformations

m : Hall current parameter

M : Hartmann magnetic number

n_e : Mass of the electrons

N : Suspension parameter

$\bar{p}$: Dimensionless pressure

P : Pressure

Q_f : Volume flow rate in fluid phase

Q_p : Volume flow rate in particulate phase

Re : Reynolds number

S : Drag coefficient

$\bar{t}$: Dimensionless time

t : Time

U_f : Longitudinal velocity in fluid phase

$\bar{u}$: Non-dimensional axial velocity

U_p : Longitudinal velocity in particulate phase

V_f : Transverse velocity in fluid phase

$\bar{v}$: Dimensionless transverse velocity

V_p : Transverse velocity in particulate phase

X, Y : Coordinate axes

$\bar{x}$: Non-dimensional axial coordinate

$\bar{y}$: Dimensionless transverse coordinate

Greek

β : Dimensionless slip parameter

δ : Dimensionless wave number

ρ_f : Density of material constituting fluid

ρ_p : Density of particulate phase

σ : Electrical conductivity

λ : Wavelength

μ_s : Viscosity coefficient

ϕ : Phase difference

λ_1 : Ratio of the relaxation and retardation times

λ_2 : Retardation time

1. INTRODUCTION

The electromagnetic properties of blood have been established for some time. The presence of hemoglobin and ionic content enables blood to respond to the imposition of electrical and magnetic fields. These features were identified in the 1930s by Pauling and co-workers at Caltech, USA [1] and have been shown to allow manipulation of both oxygenated and de-oxygenated blood flows

in many diverse applications. In the deoxygenated state, blood exhibits *paramagnetic* behavior whereas in the oxygenated state it possesses *diamagnetic* properties. Magnetic relaxation also arises in blood flow and may be of the order of several seconds. Magnetohydrodynamics (MHD) which involves the interaction of electrical/magnetic fields and electrically-conducting fluid flows has therefore emerged as a significant discipline in medical engineering. Applications include modification of light-absorbing properties of blood in biomagnetic devices [2], spinal lumbar fusion [3], pulsed therapy of tibial fractures [4] and osteoporosis treatments [5]. A significant biomedical apparatus which utilizes magnetohydrodynamics is the electromagnetic flow pump. This has been used for some years in flow meters [6], rotary maglev cardiac-assist devices [7], magnetic micro-pumps for enhanced flow control in surgical procedures [8] and also pumping of biological and chemical specimens, including DNA and saline buffers. Simulations of MHD pumps which have the advantage of generating continuous flow with low power and without moving parts, require simultaneous consideration of the fluid dynamics and electro-magnetic phenomena (Maxwell field equations). Interesting investigations in this regard include Naceur *et al.* [9] who used a finite volume solver (Ansys Fluent) to compute velocity and pressure distributions under various magnetic field loads. Hasan et al. [10] used COMSOL multiphasic modeling software to study the effects of various electromagnetic boundary conditions on magnetohydrodynamic flow in square, rectangular, circular and trapezoidal cross section micro-channel pumps. Further studies include Homsy et al. [11] for direct current high density micropumps, Vaibhayetal. [12] who also studied electro-osmotic effects, Zhao et al. [13] for alternating current MHD micropumps, Pal et al. [14] for ferrofluid thermo-magnetic micropumps, Kabbani et al. [15] for both DC and AC systems, Jian [16] for rotating EM micro-pumps. These works have generally neglected Hall current effects. Under certain magnetic field conditions with complex ionic working solutions, Hall currents can be mobilized which generate a secondary (cross) flow. This can exert a significant modification on velocity and pressure characteristics in micro-pumps [17]. Clinical verification of the contribution of Hall currents to real magnetized blood flows has also been confirmed in a number of studies including Sinatra [18] who demonstrated that Hall currents may also induce variation in magnetic field associated with the substantial magnetization of blood during slow flow and low magnetization during accelerated flow. Many investigations of Hall current effects in MHD pumping flows have been communicated using a variety of computational methods. Bég et al.[19] examined with a network

electrothermal code (PSPICE) the Hall current effects on oblique magnetohydrodynamic pumping in spinning porous media system, observing that primary flow is accelerated whereas secondary flow is inhibited with stronger Hall parameter. Lemoff and Lee [20] considered Hall current and alternating magnetic field effects on magnetohydrodynamic pumping flows with computational finite volume codes. Srnivasacharya and Shiferaw [21] employed a finite difference algorithm to investigate micropolar magnetohydrodynamic pumping with both Hall and ion slip phenomena.

An important trend in recent years in micro-pump technology has been the adoption of bio-inspired pumping mechanisms which achieve greater efficiency and sustainability. These systems employ complex biological characteristics including ciliated walls, variable stiffness and wall deformability, adaptive healing, surface tension and many other intriguing features. One of the most efficient and frequently deployed mechanisms of biological transport is *peristalsis*. This involves the propulsion of physiological fluids via rhythmic contraction of the walls of a vessel. Many sophisticated and robust peristaltic blood flow pumps have been introduced including non-occlusive designs which employ passive filling and negate negative pressure, allowing successful operation in extracorporeal circulation as described by Montoya *et al*. [22]. Computational analyses of peristaltic blood flow pumps include Natarajan and Mokhtarzadeh-Dehghan [23] who used a finite element method to simulate the hydrodynamics of "soft' two-way pulsatile peristaltic hemodynamic pumps, observing that net outflow linearly decays to zero with increasing pressure head. Lachat and Leskosek [24] developed an affinity peristaltic micro-pump for cardiopulmonary bypass procedures, noting the exceptional efficiency and sustained flow rates which can be achieved.

The magnetic properties of blood and other physiological fluids have also mobilized interest in magnetohydrodynamic peristaltic pumps. These combine the flow control abilities of MHD micropumps with the biological optimization achieved with the peristaltic mechanism, as emphasized by Pan *et al.* [25]. Tripathi and Bég [26] derived analytical solutions for transient MHD pumping with thermal diffusion in finite length channel under peristaltic waves, observing the significant regulation in velocity and pressure fields which can be achieved by combining different wave amplitudes and transverse electromagnetic body force. Kothandapani and Srinivas [27] employed a perturbation method to examine the flow characteristics in hydromagnetic peristaltic pumping in inclined channels also considering the Saffman boundary condition for porous media effects. Mekheimer [28] studied magnetic pumping of couple stress peristaltic blood

flow in non-uniform two-dimensional channels noting that an increase in Hartmann magnetic parameter enhances the pressure rise whereas greater couple-stress fluid parameter reduces it. Bhatti et al. [29] have discussed the simultaneous effects of coagulation (blood clot) and variable magnetic field on peristaltically induced motion of non-Newtonian Jeffrey nanofluid containing gyrotactic microorganism through an annulus. Ijaz et al. [30] have presented comprehensive study on the liquid and solid particles interaction propagating through a finite symmetric wavy channel with electro-osmotic flow with magnetohydrodynamics effects. Bhatti et al. [31] have given a theoretical mathematical model to determine the entropy generation on electro-kinetically modulated peristaltic propulsion on the magnetized nanofluid flow through a microchannel with joule heating. Bhatti et al. [32] have examined the effects of magnetohydrodynamics on particle-fluid suspension induced by metachronal wave. Zeeshan et al. [33] have investigated the peristaltic transport of a MHD dusty three-dimensional biorheological (Casson) fluid in a duct. These investigations generally utilized the assumption of long wavelength and low Reynolds number approximation i.e. the so-called lubrication theory. However they have neglected *wall (hydrodynamic) slip effects*. In micro-channel pumping systems, slip effects can exert a substantial influence on wall shear stress characteristics and therefore influence the velocity development across the channel span. Slip is a physical non-adherence of fluid to a boundary and can be hydrodynamic, thermal or even species-related. In MHD systems, at the walls and also in close proximity to the walls, the ions present in magnetized working fluids may also contribute to slip phenomena. Slip in viscoelastic peristaltic pumping has been addressed by Tripathi *et al*. [34] for Oldroyd-B liquids using a homotopy analytical approach. Uddin *et al.* [35] have considered both velocity and thermal slip in bioconvection nanofluid transport. Rivero and Cuevas [36] have computationally examined the effect of fluid/wall slippage in magnetohydrodynamic (MHD) micropumps in low-Hartmann-number flows, also computing the influence of slip length on the flow rate magnitudes. Further studies of slip dynamics in biological fluid mechanics include Bég et al. [37] for expanding/contracting micro-channel bio-nanoconvection flows, Bég et al. [38] for rotating disk reactor flows and Uddin et al. [39] for 3-dimensional anisotropic gyrotactic bioconvection with nano-particle doping. Slip effects in non-Newtonian peristaltic flows have been studied by El-Shehawy et al. [40] for Maxwell upper convected fluids and Ali et al. [41] for magnetic Reynolds exponential viscosity fluids.

Generally the articles quoted hitherto have simplified the blood (or biofluid) to a single phase model. Blood and indeed practically every other biological fluid contains many suspensions which are critical to functionality. These "particular" suspensions may include mucin, proteins, lipids, ions, erythrocytes, phospholipids and enzymes. These can also dramatically modify the rheology of physiological liquids. As such blood should be treated as a multi-phase medium [42]and in this context the fluid-particle suspension model provides a simple but elegant and physically realistic approximation. Fluid-particle blood flows lead to various different formulations. These may involve a simple suspension parameter introduced into momentum balance equations or Stokes particle numbers. Both approaches have been extensively deployed in recent years in peristaltic and other hemodynamic transport problems. Srivastava and Srivastava [43] obtained perturbation solutions for peristaltic pumping of a particle-fluid mixture under sinusoidal traveling wave in a two-dimensional channel, noting that critical reflux pressure is lower for the particle-fluid suspension than for the particle-free fluid and that the mean flow reversal is significantly influenced by particle concentration Bég et al. [44] used the Zhou differential transform algorithm to simulate momentum inverse Stokes number (Sk_m), particle loading parameter (p_{L}), particle-phase wall slip parameter (Ω) and other effects on blood hydrodynamics in a bio-filtration device. Chhabra and Prasad [45] performed experiments to quantify the influence of aerosol deposition in respiratory flows, showing that the introduction and clogging of aerosol particles in the acinar region can either be detrimental to gas exchange (as in the case of harmful particulate matter) or beneficial (as in the case of inhalable pharmaceuticals). Bhatti *et al*. [46] studied multi-mode heat transfer in electromagnetic pumping of viscoelastic fluid-particle suspensions in two-dimensional channels. Srivastava and Srivastava [47] examined the simultaneous Poiseuille and peristaltic transport of a particulate suspension in infinite tubes using a Frobenius series solution method and observing that mean flow is modified considerably by peristaltic wave parameter and Poiseuille's flow parameter and furthermore is damped by greater particle concentrations. Further analyses have been communicated by Medhavi and Singh[48], Kamel *et al* .[49], Bahiraei [50,51,52], Bahiraei et al. [53,54,55] the latter also addressing multi- phase flows.

In the present investigation, analytical solutions are developed for magnetohydrodynamic (MHD) pumping of fluid-particle blood suspension in a two-dimensional channel with asymmetric peristaltic waves imposed at the upper and lower walls. The Jefferys viscoelastic model is used for non-Newtonian relaxation effects. Magnetic field is imposed transverse to the channel longitudinal

axis and is sufficiently strong to invoke Hall current effects. Hydrodynamic slip is also included at the channel walls. The work is relevant to further elucidating *biological designs in magnetohydrodynamic micropumps* and extends significantly the rigid wall and simple power-law fluid study of Shahidian et al. [45]. The present simulations are *also* relevant to the magnetic pumping of viscoelastic solid-fluid mixtures by peristalsis in chemical engineering systems.

2. MATHEMATICAL MODEL

Consider the peristaltic propulsion of particulate suspension of an incompressible Jeffrey fluid through a two-dimensional asymmetric channel of width $d_1 + d_2$. Asymmetry in the channel is produced by assuming the peristaltic wave trains propagating with constant speed c along the walls to have different amplitudes and phases. The Cartesian coordinate system is adopted to describe the geometry, in such a way that $X-$ axis is taken towards the flow direction and $Y-$axis is considered towards normal along the channel (see Fig. 1). A strong static uniform magnetic field with magnetic flux density $\boldsymbol{B} = (0, 0, B_0)$ is applied in the transverse direction and is adequately large to invoke Hall current effects. The induced magnetic field is neglected by assuming a very small magnetic Reynolds number. Furthermore, it is assumed that there is no applied or polarization voltage so that the total electric field $\boldsymbol{E} = 0$. The shapes of the channel walls are represented as

$$H_1(X,t) = d_1 + a_1 \cos\left(\frac{2\pi}{\lambda}(X - ct)\right), \tag{1}$$

$$H_2(X,t) = -d_2 - a_2 \cos\left(\frac{2\pi}{\lambda}(X - ct) + \varphi\right), \tag{2}$$

where a_1 and a_2 are the wave amplitudes, λ is the wavelength, c is the velocity of propagation, t is the time and X is the direction of wave propagation. The phase difference ϕ varies in the range $0 \le \phi \le \pi$, in which $\phi = 0$ corresponds to *symmetric channel with waves out of phase* and $\phi = \pi$ corresponds to that *with waves in phase*, and further a_1, a_2, d_1, d_2 and ϕ satisfy the relation $a_1^2 + a_2^2 + 2a_1 a_2 \cos\phi \le (d_1 + d_2)^2$.

The extra stress tensor for the Jeffrey fluid model can be written as

$$\boldsymbol{\tau} = \frac{\mu_s}{1+\lambda_1}\left(\dot{\boldsymbol{D}} + \lambda_2 \ddot{\boldsymbol{D}}\right), \tag{3}$$

in which μ_s is the viscosity coefficient, λ_1 is the ratio of relaxation and retardation times, λ_2 is the retardation time, $\dot{\boldsymbol{D}}$ is the deformation tensor and $\ddot{\boldsymbol{D}}$ is the material derivative and these are given by

$$\dot{\boldsymbol{D}} = \nabla \boldsymbol{q} + (\nabla \boldsymbol{q})^T, \tag{4}$$

$$\ddot{\boldsymbol{D}} = \left(\frac{\partial}{\partial t} + \boldsymbol{q} \bullet \nabla \right) \dot{\boldsymbol{D}}. \tag{5}$$

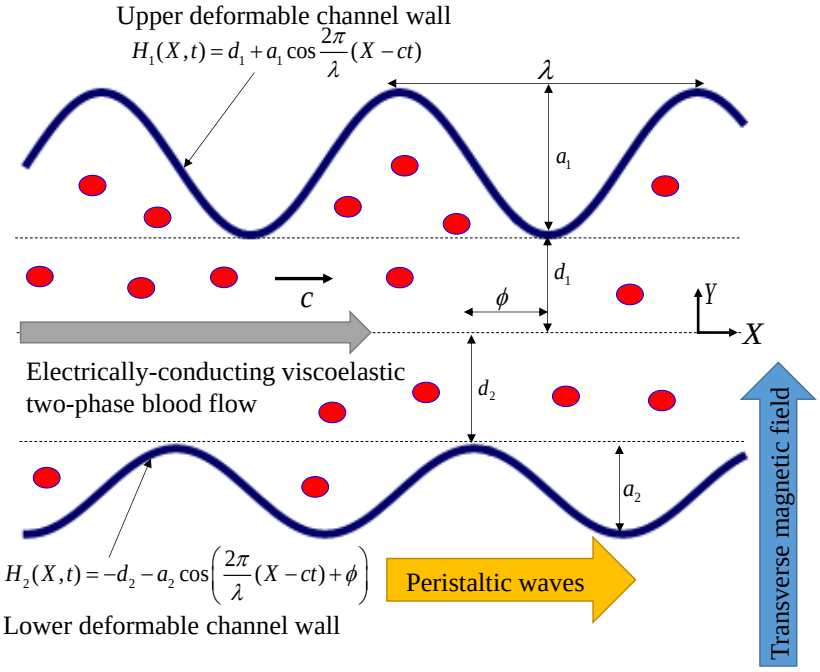

Fig.1: Geometric model.

The Jeffreys model arises naturally for polymer solutions if one decomposes the total stress into a Newtonian viscous stress for the solvent and an additional stress for the polymer. It was introduced for polymeric suspensions but has shown significant promise for multi-phase blood flows. The Jeffrey model is in fact a three-parameter viscoelastic model and as such more refined than the Maxwell model. It augments the time derivative of the shear rate tensor in the Maxwell model by supplementing the stress relaxation time with a retardation time [46].

The two-phase blood flow considered is electrically-conducting and magnetohydrodynamic effects are therefore invoked. The walls of the channel are considered to be electrically-insulated. The generalized Ohm's law can be written as [64]

$$\boldsymbol{J} = \sigma\left(\boldsymbol{E} + \boldsymbol{q}\times\boldsymbol{B} - \frac{1}{en_e}\left(\boldsymbol{J}\times\boldsymbol{B}\right)\right), \tag{6}$$

where n_e the mass of the electron and e is the charge of the ions. Equation (6) can be solved in J to yield the Lorentz body force vector in the form [64]

$$\boldsymbol{J}\times\boldsymbol{B} = \frac{-\sigma B_0^2}{1+m^2}\left[\left(U - mV\right)i + \left(mU + V\right)j\right], \tag{7}$$

where U and V are components of the velocity vector and $m = \frac{\sigma B_0}{en_e}$ is the Hall current parameter.

Within the framework of continuum mechanics, the equations governing the unsteady conservation equations for mass and linear momentum for both fluid and particle phase are expressed as follows [65, 66]:

Fluid phase

$$\frac{\partial U_f}{\partial X} + \frac{\partial V_f}{\partial Y} = 0, \tag{8}$$

$$\left(1-C\right)\rho_f\left(\frac{\partial U_f}{\partial t} + U_f\frac{\partial U_f}{\partial X} + V_f\frac{\partial U_f}{\partial Y}\right) = -\left(1-C\right)\frac{\partial P}{\partial X} + \left(1-C\right)\left(\frac{\partial \tau_{XX}}{\partial X} + \frac{\partial \tau_{XY}}{\partial Y}\right) + CS\left(U_p - U_f\right) - \left(1-C\right)\frac{\sigma B_0^2}{1+m^2}\left(U - mV\right), \tag{9}$$

$$\left(1-C\right)\rho_f\left(\frac{\partial V_f}{\partial t} + U_f\frac{\partial V_f}{\partial X} + V_f\frac{\partial V_f}{\partial Y}\right) = -\left(1-C\right)\frac{\partial P}{\partial Y} + \left(1-C\right)\left(\frac{\partial \tau_{YX}}{\partial X} + \frac{\partial \tau_{YY}}{\partial Y}\right) + CS\left(V_p - V_f\right) - \left(1-C\right)\frac{\sigma B_0^2}{1+m^2}\left(mU + V\right). \tag{10}$$

Particulate phase

$$\frac{\partial U_p}{\partial X} + \frac{\partial V_p}{\partial Y} = 0, \tag{11}$$

$$C\rho_p\left(\frac{\partial U_p}{\partial t} + U_p\frac{\partial U_p}{\partial X} + V_p\frac{\partial U_p}{\partial Y}\right) = -C\frac{\partial P}{\partial X} + CS\left(U_f - U_p\right), \tag{12}$$

$$C\rho_p\left(\frac{\partial V_p}{\partial t} + U_p\frac{\partial V_p}{\partial X} + V_p\frac{\partial V_p}{\partial Y}\right) = -C\frac{\partial P}{\partial Y} + CS\left(V_f - V_p\right), \tag{13}$$

where X and Y are Cartesian coordinates with X is measured in the direction of wave propagation and Y is measured in the transverse direction of the channel walls, (U_f, V_f) denotes fluid phase velocities, (U_p, V_p) denotes particulate phase velocities, ρ_f and ρ_p are the actual densities of the materials constituting fluid and particulate phase respectively, $(1-C)\rho_f$ is the fluid phase density, $C\rho_p$ is the particulate phase density, P is the pressure, C denotes the volume fraction density of the particles, $\mu_s(C)$ is the particle-fluid mixture viscosity and S the drag coefficient of interaction for the force exerted by one phase on the other. The *drag coefficient* expression for the present problem is selected as [65, 66]

$$S = \frac{9\mu_0}{2\breve{a}^2}\lambda(C), \quad \lambda(C) = \frac{4+3\sqrt{8C-3C^2}+3C}{(2-3C)^2}, \tag{14}$$

in which, μ_0 is the fluid viscosity and $\breve{a}$ is the radius of the particle. Many empirical relations have been suggested to express the viscosity of the suspension as a function of particle concentration and viscosity of the suspending medium. Einstein was the first to showtheoretically that the viscosity of the suspension μ_s was related to that of the suspending medium μ_0 for spheres in suspension by $\mu_0 = \mu_s(1-2.5C)$. However, the Einstein formula expresses the viscosity of the suspension only when C is less than 0.05. As C increases from 0.05, the suspension viscosity deviates from Einstein's equation, as elaborated by Landau and Lifschitz[47].For the present problem, an empirical relation for the viscosity of the suspension is as follows:

$$\mu_s = \frac{\mu_0}{1-\chi C}, \quad \chi = 0.07\exp\left(2.49C + \frac{1107}{T}\exp(-1.69C)\right), \tag{15}$$

where T is the absolute temperature. The viscosity of the suspension expressed by this formula is found to be reasonably accurate up to $C = 0.6$. Charmand Kurland [48] tested the equation (15) with a cone and plate viscometer and found it to be within ten percent agreement of blood suspensions. To eliminate the time dimension from the mathematical model, it is convenient to define the transformation variable from the fixed frame to the wave (laboratory) frame

$$x = X - ct,\ y = Y,\ u_{f,p}(x,y) = U_{f,p}(X,Y,t) - c,\ v_{f,p}(x,y) = V_{f,p}(X,Y,t),\ p(x,y) = p(X,Y,t). \tag{16}$$

Using the above transformations, the governing partial differential equations in the wave frame for both fluid and particulate phaseassume the form:

Fluid phase

$$\frac{\partial u_f}{\partial x}+\frac{\partial v_f}{\partial y}=0, \tag{17}$$

$$(1-C)\rho_f\left(u_f\frac{\partial u_f}{\partial x}+v_f\frac{\partial u_f}{\partial y}\right)=-(1-C)\frac{\partial p}{\partial x}+(1-C)\left(\frac{\partial \tau_{xx}}{\partial x}+\frac{\partial \tau_{xy}}{\partial y}\right)+CS\left(u_p-u_f\right)$$
$$-(1-C)\frac{\sigma B_0^2}{1+m^2}(u+c-mv), \tag{18}$$

$$(1-C)\rho_f\left(u_f\frac{\partial v_f}{\partial x}+v_f\frac{\partial v_f}{\partial y}\right)=-(1-C)\frac{\partial p}{\partial y}+(1-C)\left(\frac{\partial \tau_{yx}}{\partial x}+\frac{\partial \tau_{yy}}{\partial y}\right)+CS\left(v_p-v_f\right)$$
$$-(1-C)\frac{\sigma B_0^2}{1+m^2}\left(m(u+c)+v\right), \tag{19}$$

Particulate phase

$$\frac{\partial u_p}{\partial x}+\frac{\partial v_p}{\partial y}=0, \tag{20}$$

$$C\rho_p\left(u_p\frac{\partial u_p}{\partial x}+v_p\frac{\partial u_p}{\partial y}\right)=-C\frac{\partial p}{\partial x}+CS\left(u_f-u_p\right), \tag{21}$$

$$C\rho_p\left(u_p\frac{\partial v_p}{\partial x}+v_p\frac{\partial v_p}{\partial y}\right)=-C\frac{\partial p}{\partial y}+CS\left(v_f-v_p\right), \tag{22}$$

It is further advantageous to normalize the conservation equations to circumvent the need for actual material properties of multi-phase blood. The following dimensionless parameters are therefore defined:

$$\bar{x}=\frac{x}{\lambda},\ \bar{y}=\frac{y}{d_1},\ \bar{u}=\frac{u}{c},\ \bar{v}=\frac{v}{\delta c},\ h_1=\frac{H_1}{a_1},\ h_2=\frac{H_2}{d_1},\ \bar{t}=\frac{ct}{\lambda},\ \bar{p}=\frac{d_1^2 p}{\lambda\mu_s c},\ \delta=\frac{d_1}{\lambda},\ d=\frac{d_2}{d_1},$$
$$a=\frac{a_1}{d_1},\ b=\frac{a_2}{d_1},\ \mathrm{Re}=\frac{\rho c d_1}{\mu_s},\ M=\sqrt{\frac{\sigma}{\mu_s}}B_0 d_1,\ \bar{\tau}=\frac{d_1\tau}{\mu_s c},\ N=\frac{Sd_1^2}{\mu_s}, \tag{23}$$

Here $\bar{x}$ is dimensionless longitudinal (axial) coordinate, $\bar{y}$ is dimensionless transverse coordinate, $\bar{u}$ is dimensionless axial velocity, $\bar{v}$ is dimensionless transverse velocity, h_1 and h_2 are non-dimensional wall deformations, $\bar{t}$ is dimensionless time, $\bar{p}$ is dimensionless pressure, δ is

dimensionless wave number, *d* is dimensionless channel width ratio, *a* is amplitude ratio of the upper wall wave, *b* is amplitude ratio of the lower wall wave, *Re* is the Reynolds number, M denotes Hartmann number, $\bar{\tau}$ is non-dimensional relaxation time and N is the suspension parameter. Using the above non-dimensional quantities in the equations (17)-(22), and invoking the long wavelength and low Reynolds number approximations, the resulting equations for fluid phase and particulate phases emerge as:

$$\frac{dp}{dx} = \frac{1}{1+\lambda_1}\frac{\partial^2 u_f}{\partial y^2} - \frac{M^2}{1+m^2}\left(u_f + 1\right) + \frac{NC}{\left(1-C\right)}\left(u_p - u_f\right), \tag{24a}$$

$$\frac{dp}{dx} = N\left(u_f - u_p\right), \tag{24b}$$

The corresponding dimensionless boundary conditions take the form:

$$u_f + \frac{\beta}{1+\lambda_1}\frac{\partial u_f}{\partial y} = -1 \quad \text{at} \quad y = h_1, \tag{25}$$

$$u_f - \frac{\beta}{1+\lambda_1}\frac{\partial u_f}{\partial y} = -1 \quad \text{at} \quad y = h_2. \tag{26}$$

in the above expressions, λ_1 is the viscoelastic parameter and $\beta\left(=\frac{\gamma}{d_1}\right)$ is the non-dimensional slip parameter.

3. ANALYTICAL SOLUTIONS

Using Eqns. (24a,b), with the corresponding boundary conditions (25) and (26), the exact solutions for the axial velocities for the fluid phase and particulate phase are:

$$u_f = -1 + \frac{dp}{dx}\left(C_1\cosh\left(M_1 y\right) + C_2\sinh\left(M_1 y\right) - \frac{1+\lambda_1}{M_1^2\left(1-C\right)}\right), \tag{27}$$

$$u_p = -1 + \frac{dp}{dx}\left(C_1\cosh\left(M_1 y\right) + C_2\sinh\left(M_1 y\right) - \frac{1+\lambda_1}{M_1^2\left(1-C\right)} - \frac{1}{N}\right). \tag{28}$$

where

$$M_1 = \sqrt{\left(1+\lambda_1\right)\left(\frac{M^2}{1+m^2} + \frac{1}{Da}\right)},$$

$$C_1 = \frac{(1+\lambda_1)^2\left((1+\lambda_1)(\sinh(M_1h_1)-\sinh(M_1h_2))+\beta M_1(\cosh(M_1h_2)+\cosh(M_1h_1))\right)}{M_1^2(1-C)\left(\left((1+\lambda_1)^2+\beta^2M_1^2\right)\sinh(M_1(h_1-h_2))+2\beta M_1(1+\lambda_1)\cosh(M_1(h_1-h_2))\right)},$$

$$C_2 = \frac{(1+\lambda_1)^2\left((1+\lambda_1)(\cosh(M_1h_2)-\cosh(M_1h_1))-\beta M_1(\sinh(M_1h_2)+\sinh(M_1h_1))\right)}{M_1^2(1-C)\left(\left((1+\lambda_1)^2+\beta^2M_1^2\right)\sinh(M_1(h_1-h_2))+2\beta M_1(1+\lambda_1)\cosh(M_1(h_1-h_2))\right)}.$$

For the fluid and particle phases, the *volumetric flow rate*is written as

$$Q_f = (1-C)\int_{h_2}^{h_1} u_f\, dy, \tag{29}$$

$$Q_p = C\int_{h_2}^{h_1} u_p\, dy, \tag{30}$$

The *total volumetric flow rate* is therefore simply given by:

$$Q = Q_f + Q_p. \tag{31}$$

Using the equations (29) and (30) in the equation (31), we get

$$Q = (h_2-h_1) - \frac{1}{M_1}\frac{dp}{dx}\left(\begin{array}{l} C_1(\sinh(M_1h_1)-\sinh(M_1h_2))+C_2(\cosh(M_1h_1)-\cosh(M_1h_2)) \\ +\dfrac{(1+\lambda_1+CM_1^2)}{M_1(1-C)}(h_2-h_1)\end{array}\right). \tag{32}$$

The pressure gradient dp/dx is calculated with the help of above equation, it can be written as

$$\frac{dp}{dx} = \frac{M_1^2(1-C)(h_2-h_1-Q)}{\left(\begin{array}{l} M_1(1-C)(C_1(\sinh(M_1h_1)-\sinh(M_1h_2))+C_2(\cosh(M_1h_1)-\cosh(M_1h_2))) \\ +(1+\lambda_1+CM_1^2)(h_2-h_1)\end{array}\right)}. \tag{33}$$

The *dimensionless form for pressure rise* is evaluated numerically using the following formula:

$$\Delta p_\lambda = \int_0^1 \left(\frac{dp}{dx}\right) dx. \tag{34}$$

The expression for *dimensionless stream function* satisfying equation of continuity is defined as

$$u_{f,p} = \frac{\partial \psi_{f,p}}{\partial y}, \quad v_{f,p} = -\frac{\partial \psi_{f,p}}{\partial x}, \tag{35}$$

4. NUMERICAL RESULTS AND INTERPRETATION

In this section, selected graphical results for the influence of different parameters on the fluid phase and particulate phase are elaborated. We consider the effects of volume fraction density, Hall current parameter, wall slip, viscoelastic parameter, suspension parameter and Hartmann number on fluid velocity, particulate velocity, fluid/particle fluid and particulate volumetric flow rates,

axial pressure gradient, pressure rise, skin friction distribution and streamline distributions. The expression for pressure rise i.e. eqn. (34) is evaluated numerically. Selected results are depicted in **Figs 2-9.**

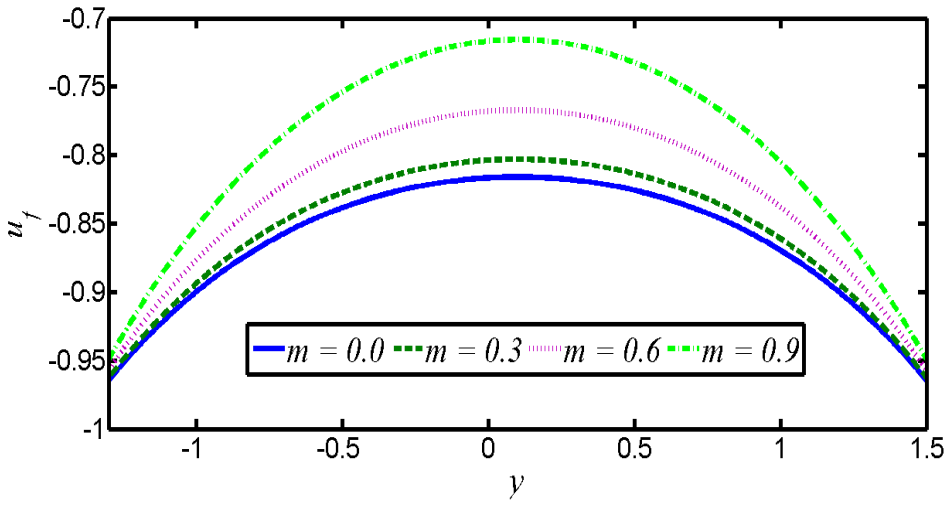

(a)

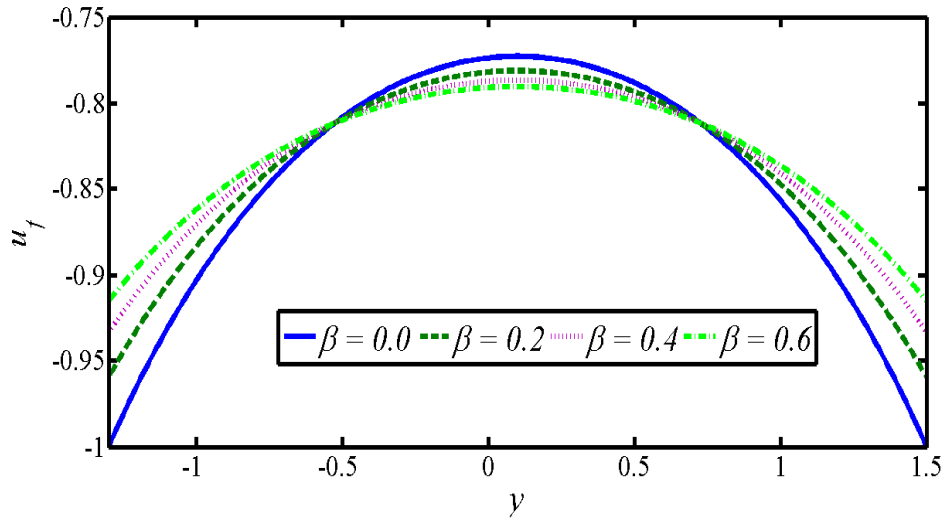

(b)

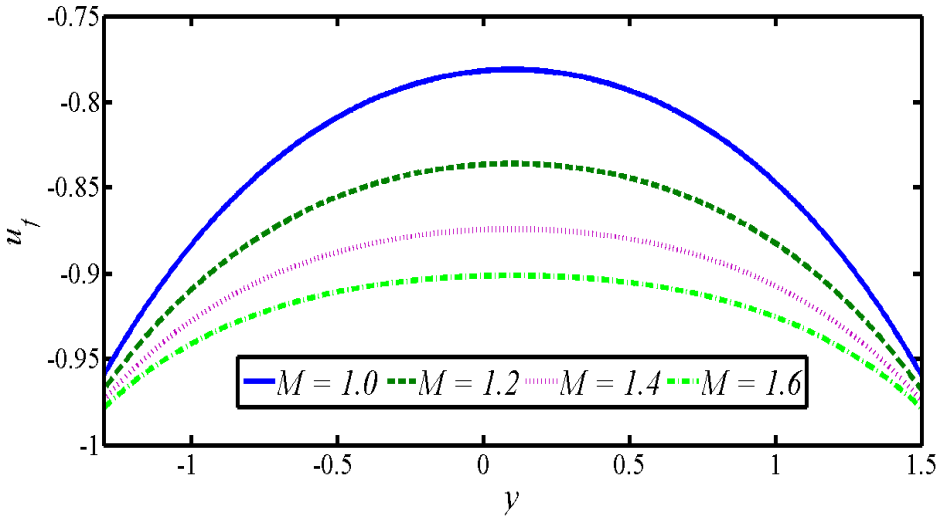
-0.75
-0.8
-0.85
-0.9
-0.95
-1
u_f
-1
-0.5
0
0.5
1
1.5
y
$M = 1.0$
$M = 1.2$
$M = 1.4$
$M = 1.6$

(c)

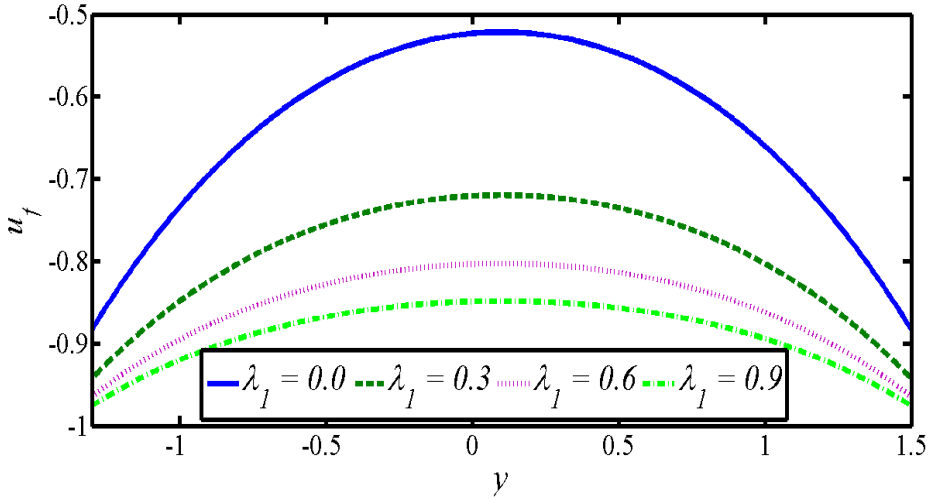
-0.5
-0.6
-0.7
-0.8
-0.9
-1
u_f
-1
-0.5
0
0.5
1
1.5
y
$\lambda_1 = 0.0$
$\lambda_1 = 0.3$
$\lambda_1 = 0.6$
$\lambda_1 = 0.9$

(d)

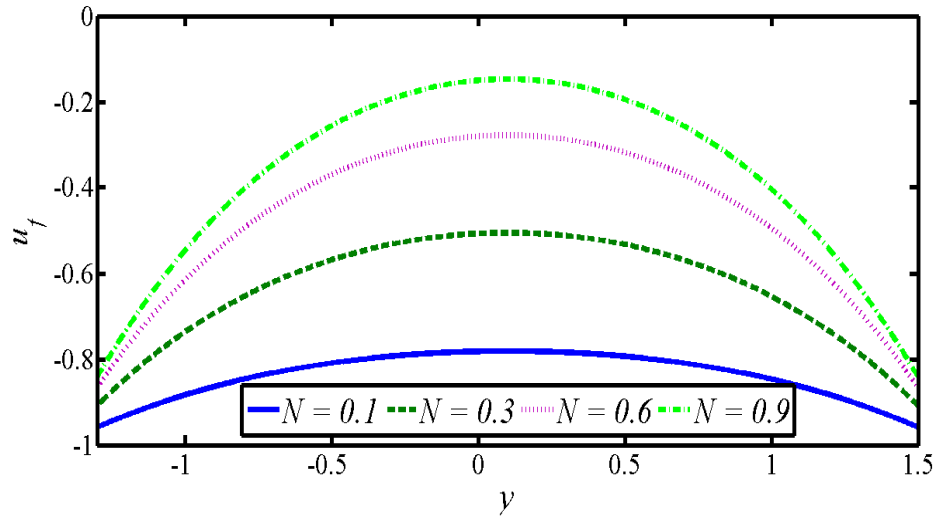

(e)

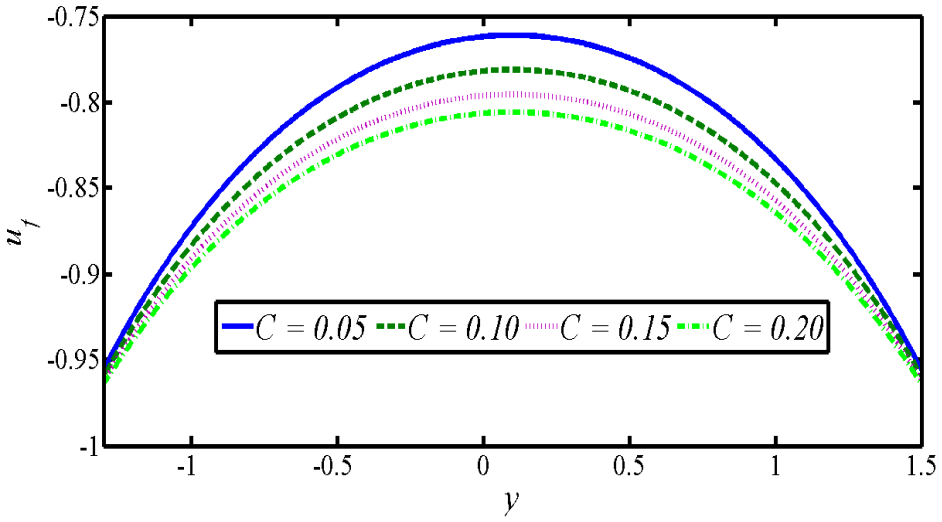

(f)

Figure 2: Effects of different fluid parameters on the velocity profile in the fluid phase for $(a)\ a = 0.5, b = 0.6, d = 1, x = 1, M = 1, \beta = 0.2, \phi = \pi/3, Q = 2, C = 0.1, \lambda_1 = 0.5, N = 0.1,$ $(b)\ a = 0.5, b = 0.6, d = 1, x = 1, M = 1, \phi = \pi/3, Q = 2, C = 0.1, \lambda_1 = 0.5, N = 0.1, m = 0.5,$ $(c)\ a = 0.5, b = 0.6, d = 1, x = 1, \beta = 0.2, \phi = \pi/3, Q = 2, C = 0.1, \lambda_1 = 0.5, N = 0.1, m = 0.5,$ $(d)\ a = 0.5, b = 0.6, d = 1, x = 1, M = 1, \beta = 0.2, \phi = \pi/3, Q = 2, C = 0.1, N = 0.1, m = 0.5,$ $(e)\ a = 0.5, b = 0.6, d = 1, x = 1, M = 1, \beta = 0.2, \phi = \pi/3, Q = 2, C = 0.1, \lambda_1 = 0.5, m = 0.5,$ $(f)\ a = 0.5, b = 0.6, d = 1, x = 1, M = 1, \beta = 0.2, \phi = \pi/3, Q = 2, \lambda_1 = 0.5, N = 0.1, m = 0.5.$

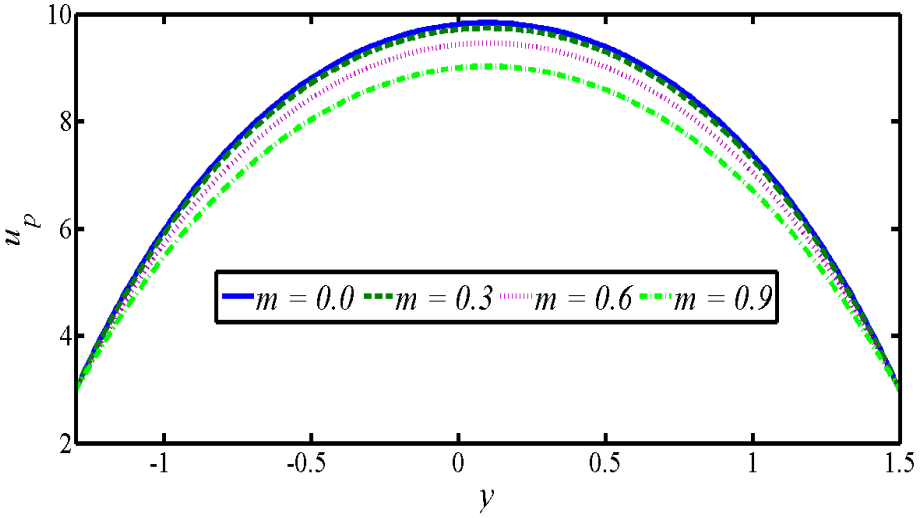
10
8
6
4
2
u_p
$m = 0.0$ $m = 0.3$ $m = 0.6$ $m = 0.9$
-1
-0.5
0
0.5
1
1.5
y

(a)

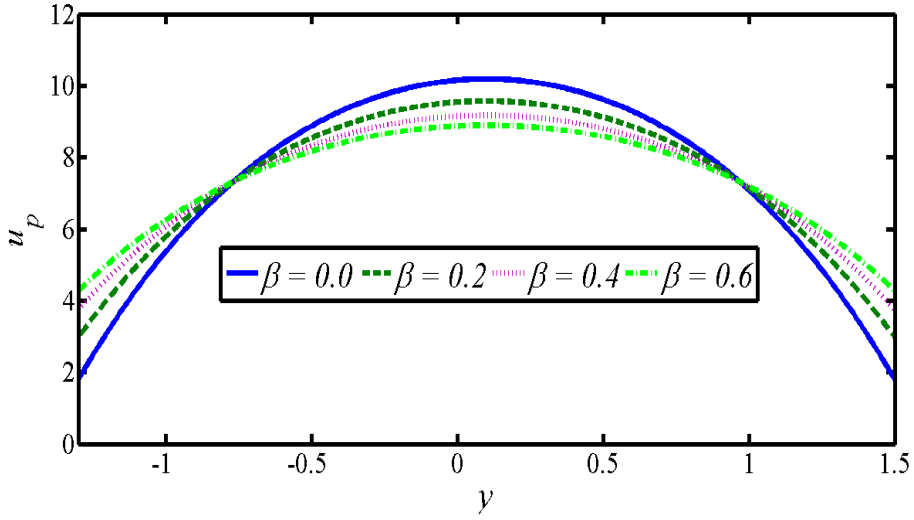
12
10
8
6
4
2
0
u_p
$\beta = 0.0$ $\beta = 0.2$ $\beta = 0.4$ $\beta = 0.6$
-1
-0.5
0
0.5
1
1.5
y

(b)

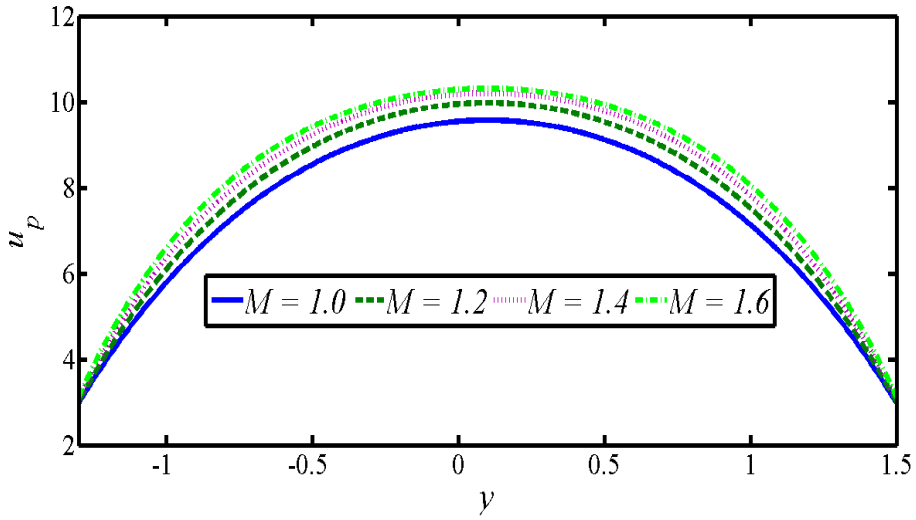
12
10
8
6
4
2
u_p
-1
-0.5
0
0.5
1
1.5
y
$M = 1.0$
$M = 1.2$
$M = 1.4$
$M = 1.6$

(c)

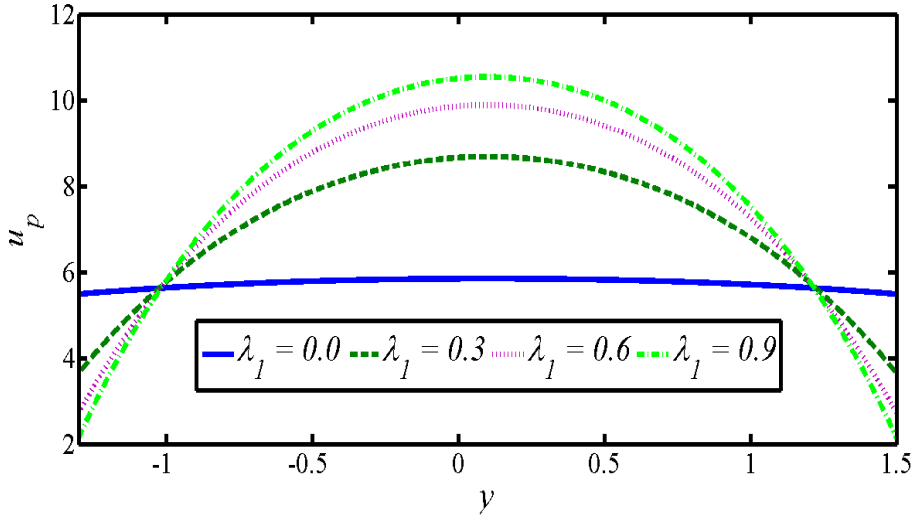
12
10
8
6
4
2
u_p
-1
-0.5
0
0.5
1
1.5
y
$\lambda_1 = 0.0$
$\lambda_1 = 0.3$
$\lambda_1 = 0.6$
$\lambda_1 = 0.9$

(d)

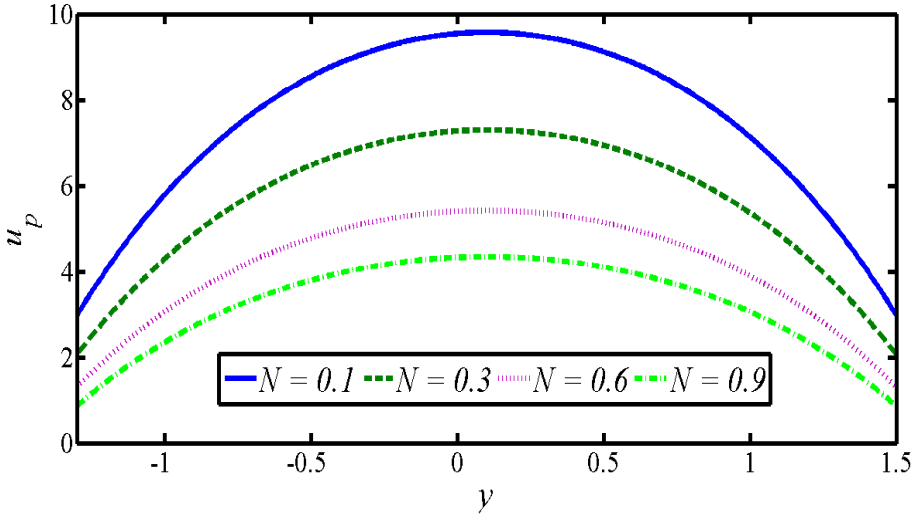

(e)

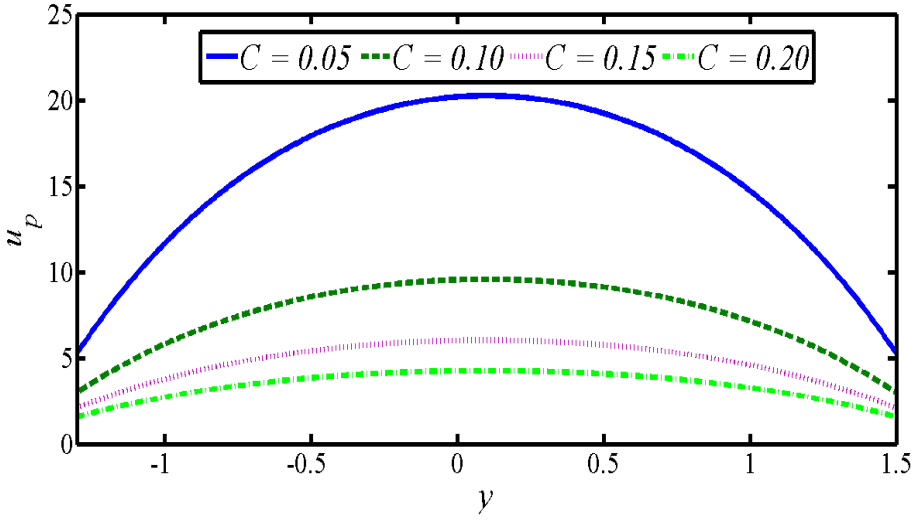

(f)

Figure 3: Effects of different fluid parameters on the velocity profile in the particulate phase for $(a)\ a = 0.5, b = 0.6, d = 1, x = 1, M = 1, \beta = 0.2, \phi = \pi/3, Q = 2, C = 0.1, \lambda_1 = 0.5, N = 0.1,\ (b)\ a = 0.5, b = 0.6, d = 1, x = 1, M = 1, \phi = \pi/3, Q = 2, C = 0.1, \lambda_1 = 0.5, N = 0.1, m = 0.5,\ (c)\ a = 0.5, b = 0.6, d = 1, x = 1, \beta = 0.2, \phi = \pi/3, Q = 2, C = 0.1, \lambda_1 = 0.5, N = 0.1, m = 0.5,\ (d)\ a = 0.5, b = 0.6, d = 1, x = 1, M = 1, \beta = 0.2, \phi = \pi/3, Q = 2, C = 0.1, N = 0.1, m = 0.5,\ (e)\ a = 0.5, b = 0.6, d = 1, x = 1, M = 1, \beta = 0.2, \phi = \pi/3, Q = 2, C = 0.1, \lambda_1 = 0.5, m = 0.5,\ (f)\ a = 0.5, b = 0.6, d = 1, x = 1, M = 1, \beta = 0.2, \phi = \pi/3, Q = 2, \lambda_1 = 0.5, N = 0.1, m = 0.5.$

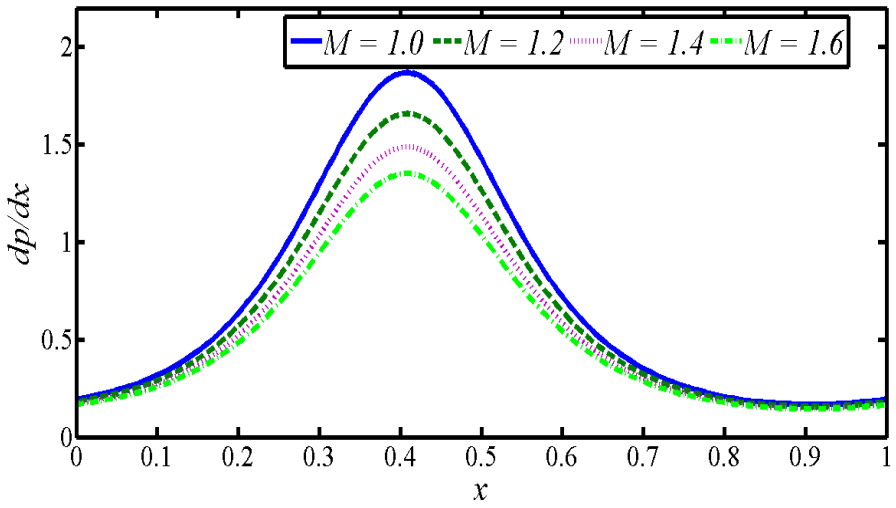
M = 1.0
M = 1.2
M = 1.4
M = 1.6
dp/dx
x
0
0.5
1
1.5
2
0.1
0.2
0.3
0.4
0.5
0.6
0.7
0.8
0.9

(a)

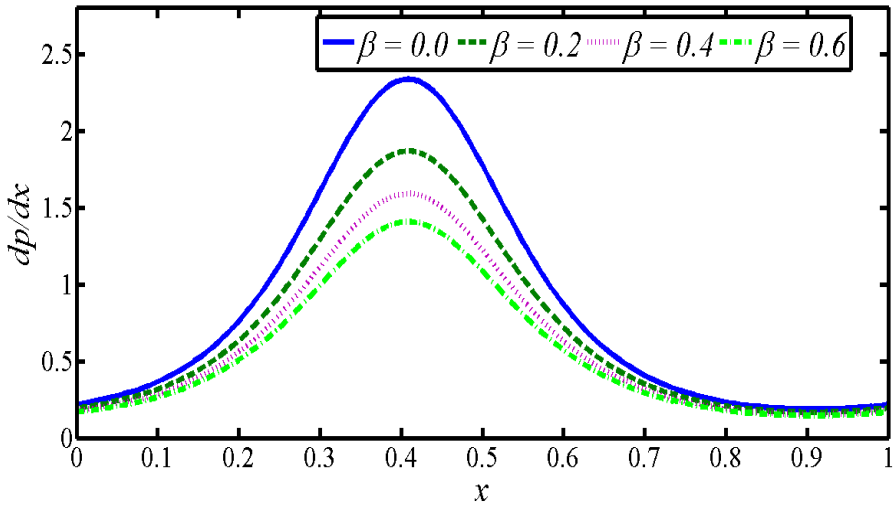
β = 0.0
β = 0.2
β = 0.4
β = 0.6
dp/dx
x
0
0.5
1
1.5
2
2.5
0.1
0.2
0.3
0.4
0.5
0.6
0.7
0.8
0.9

(b)

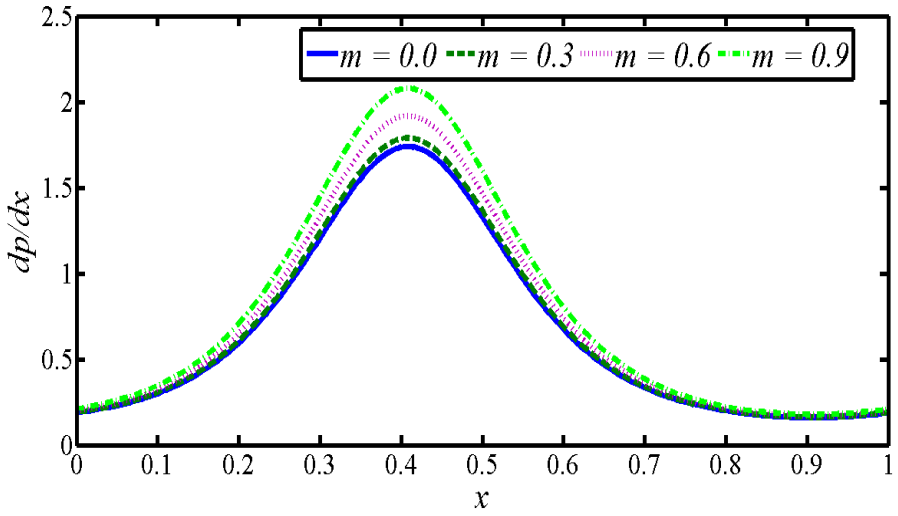
m = 0.0
m = 0.3
m = 0.6
m = 0.9
dp/dx
x
0
0.5
1
1.5
2
2.5
0.1
0.2
0.3
0.4
0.5
0.6
0.7
0.8
0.9

(c)

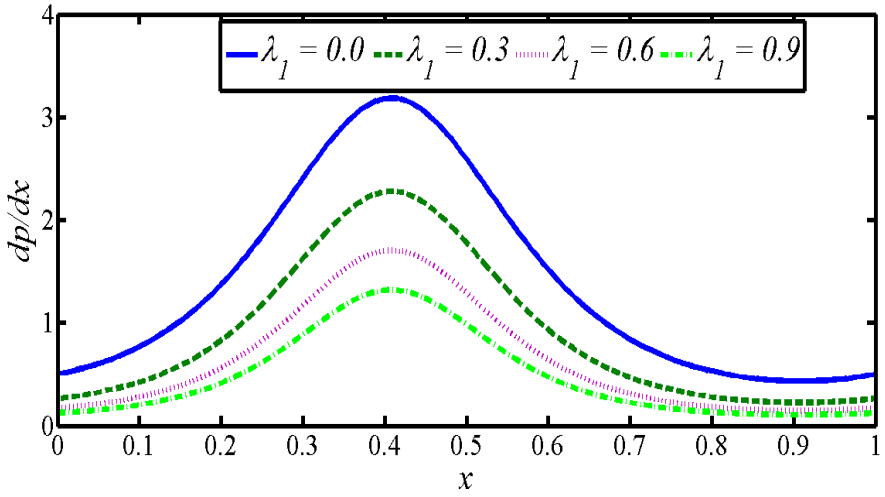
λ1 = 0.0
λ1 = 0.3
λ1 = 0.6
λ1 = 0.9
dp/dx
x
0
1
2
3
4
0.1
0.2
0.3
0.4
0.5
0.6
0.7
0.8
0.9

(d)

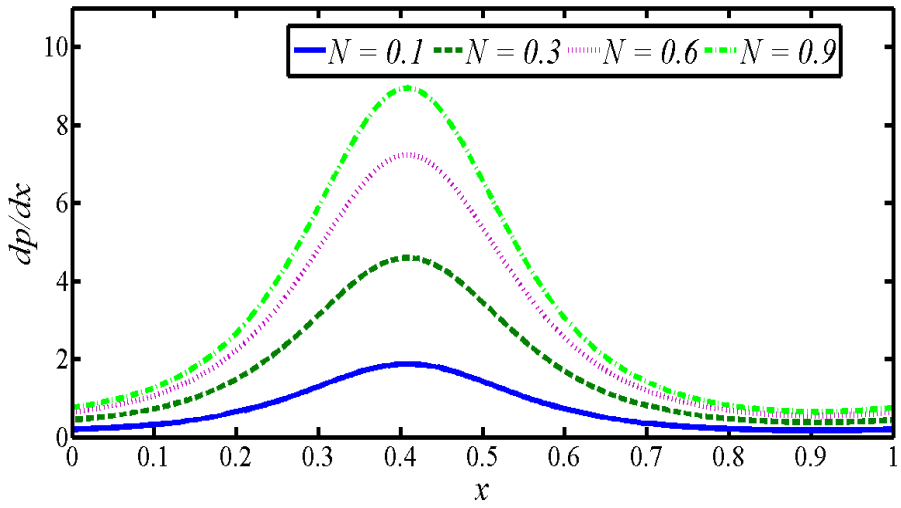

(e)

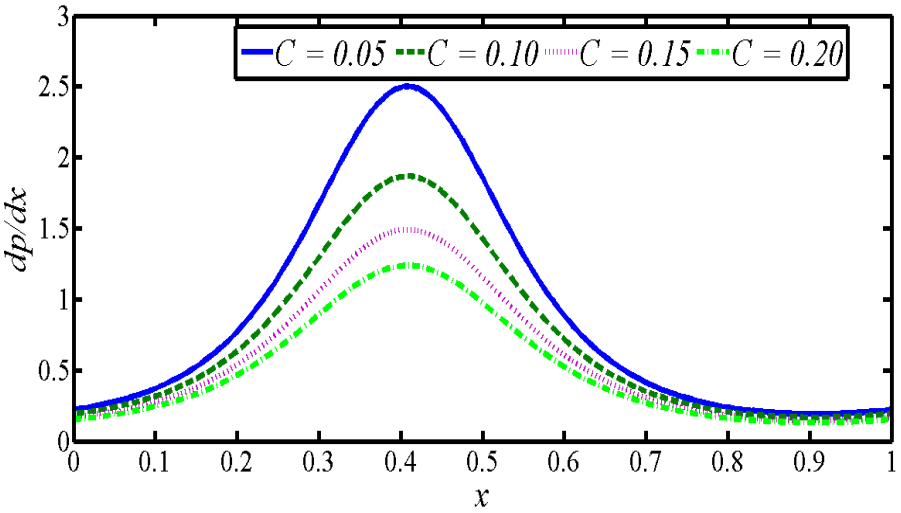

(f)

Figure 4: Effects of different fluid parameters on the pressure gradient for $(a)\ a=0.5, b=0.6, d=1, y=0, \beta=0.2, \phi=\pi/3, Q=-3, C=0.1, \lambda_1=0.5, N=0.1, m=0.5, (b)\ a=0.5, b=0.6, d=1, y=0, M=1, \phi=\pi/3, Q=-3, C=0.1, \lambda_1=0.5, N=0.1, m=0.5, (c)\ a=0.5, b=0.6, d=1, y=0, M=1, \beta=0.2, \phi=\pi/3, Q=-3, C=0.1, \lambda_1=0.5, N=0.1,\ (d)\ a=0.5, b=0.6, d=1, y=0, M=1, \beta=0.2, \phi=\pi/3, Q=-3, C=0.1, N=0.1, m=0.5, (e)\ a=0.5, b=0.6, d=1, y=0, M=1, \beta=0.2, \phi=\pi/3, Q=-3, C=0.1, \lambda_1=0.5, m=0.5, (f)\ a=0.5, b=0.6, d=1, y=0, M=1, \beta=0.2, \phi=\pi/3, Q=-3, \lambda_1=0.5, N=0.1, m=0.5.$

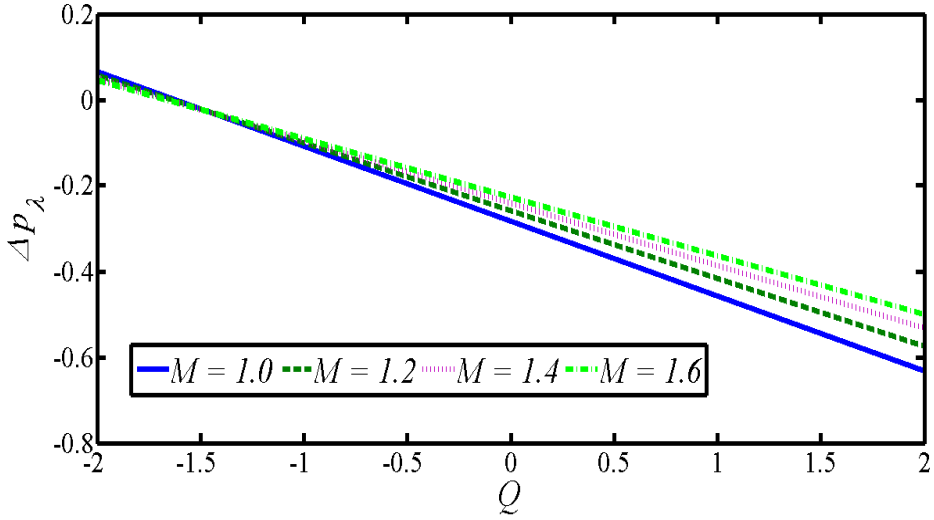
0.2
0
-0.2
-0.4
-0.6
-0.8
Δp_λ
-2
-1.5
-1
-0.5
0
0.5
1
1.5
2
Q
$M = 1.0$
$M = 1.2$
$M = 1.4$
$M = 1.6$

(a)

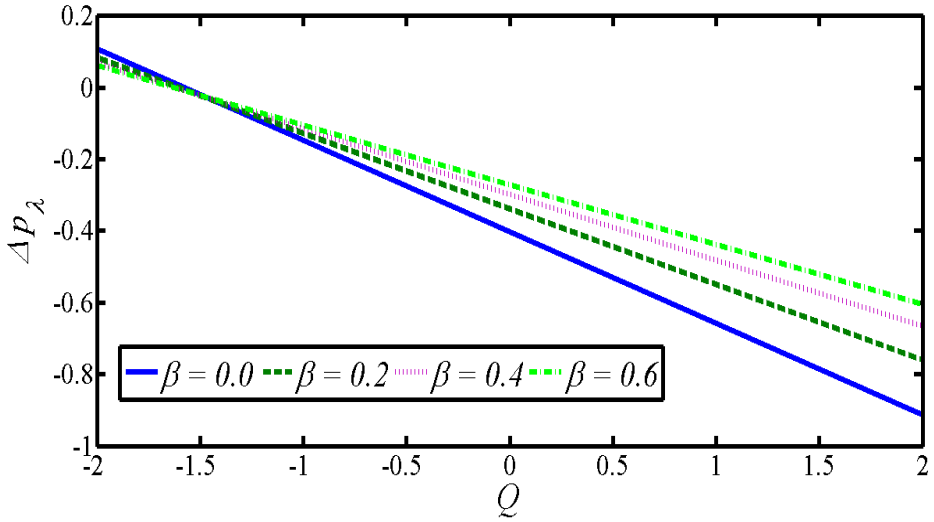
0.2
0
-0.2
-0.4
-0.6
-0.8
-1
Δp_λ
-2
-1.5
-1
-0.5
0
0.5
1
1.5
2
Q
$\beta = 0.0$
$\beta = 0.2$
$\beta = 0.4$
$\beta = 0.6$

(b)

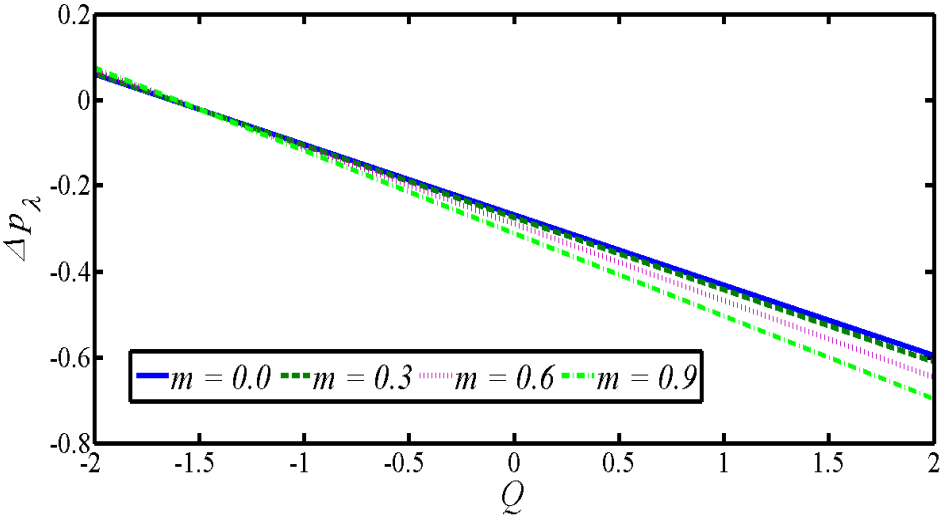
0.2
0
-0.2
-0.4
-0.6
-0.8
-2
-1.5
-1
-0.5
0
0.5
1
1.5
2
Δp_λ
Q
$m = 0.0$
$m = 0.3$
$m = 0.6$
$m = 0.9$

(c)

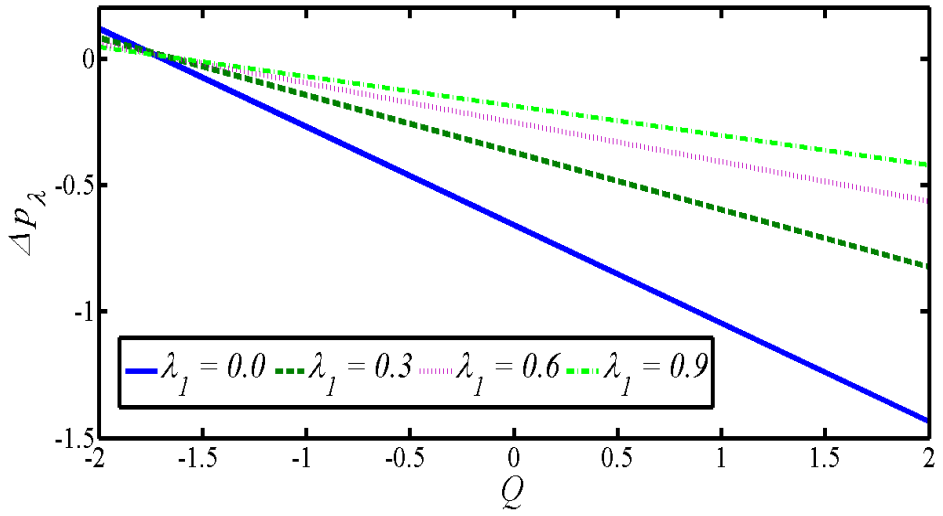
0
-0.5
-1
-1.5
-2
-1.5
-1
-0.5
0
0.5
1
1.5
2
Δp_λ
Q
$\lambda_1 = 0.0$
$\lambda_1 = 0.3$
$\lambda_1 = 0.6$
$\lambda_1 = 0.9$

(d)

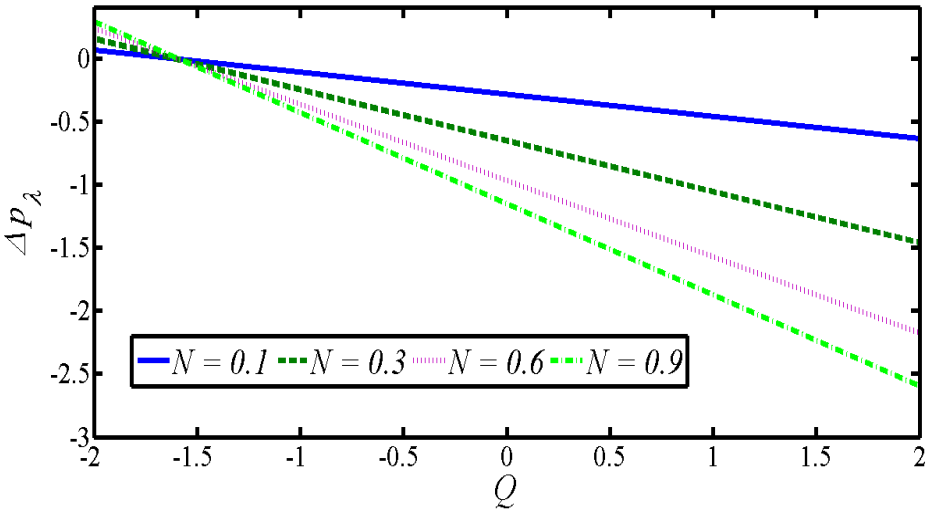

(e)

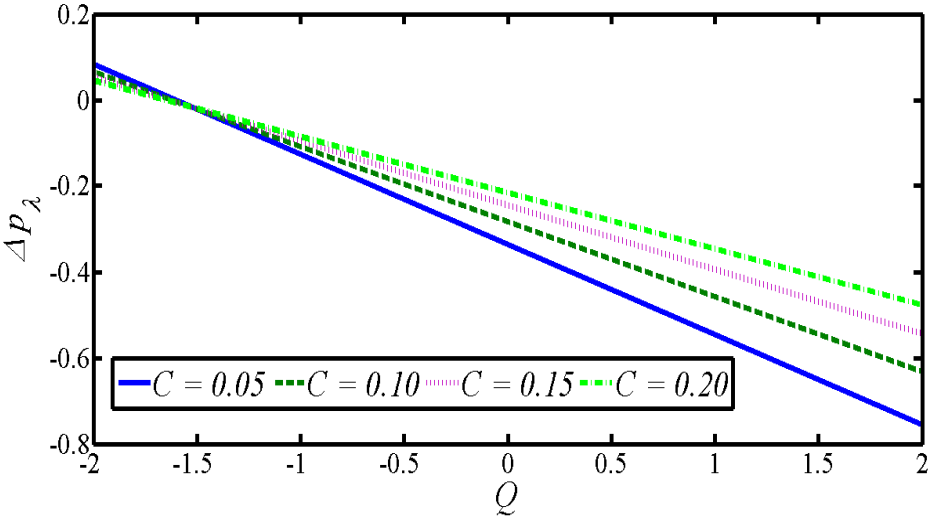

(f)

Figure 5: Effects of different fluid parameters on the pressure rise for $(a)\ a = 0.5, b = 0.6, d = 1, y = 0, \beta = 0.5, \phi = \pi/3, C = 0.1, \lambda_1 = 0.5, N = 0.1, m = 0.5, (b)\ a = 0.5, b = 0.6, d = 1, y = 0, \phi = \pi/3, C = 0.1, \lambda_1 = 0.5, N = 0.1, m = 0.5, M = 1, (c)\ a = 0.5, b = 0.6, d = 1, y = 0, \beta = 0.5, \phi = \pi/3, C = 0.1, \lambda_1 = 0.5, N = 0.1, M = 1, (d)\ a = 0.5, b = 0.6, d = 1, y = 0, \beta = 0.5, \phi = \pi/3, C = 0.1, N = 0.1, m = 0.5, M = 1, (e)\ a = 0.5, b = 0.6, d = 1, y = 0, \beta = 0.5, \phi = \pi/3, C = 0.1, \lambda_1 = 0.5, m = 0.5, M = 1, (f)\ a = 0.5, b = 0.6, d = 1, y = 0, \beta = 0.5, \phi = \pi/3, \lambda_1 = 0.5, N = 0.1, m = 0.5, M = 1.$

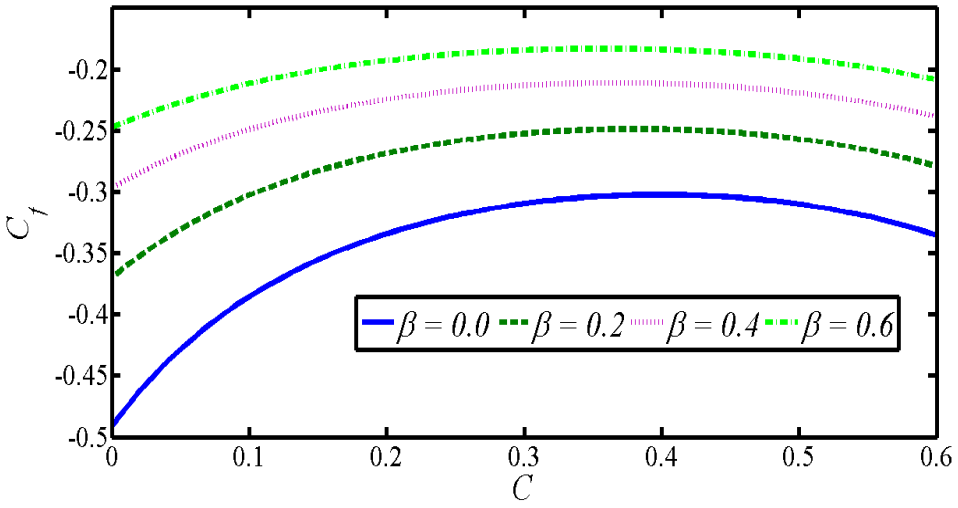
-0.2
-0.25
-0.3
-0.35
-0.4
-0.45
-0.5
C_f
0
0.1
0.2
0.3
0.4
0.5
0.6
C
$\beta = 0.0$
$\beta = 0.2$
$\beta = 0.4$
$\beta = 0.6$

(a)

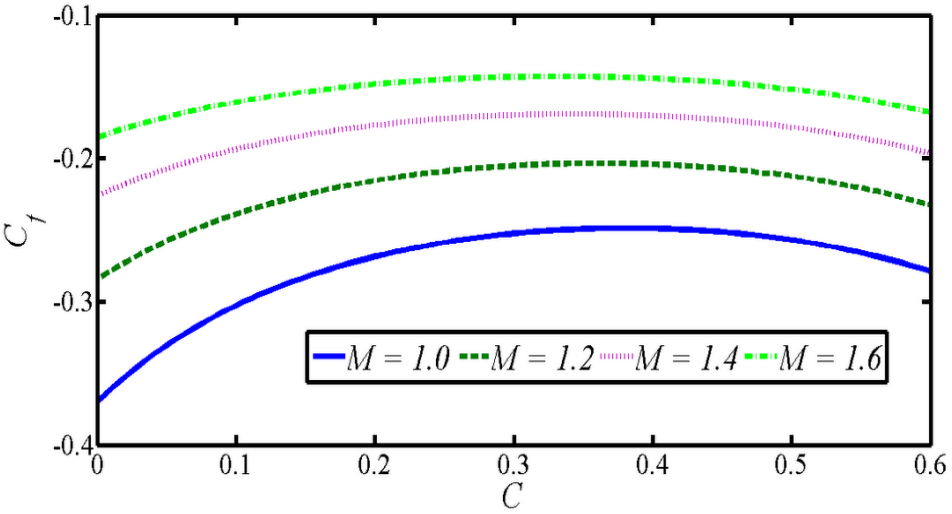
-0.1
-0.2
-0.3
-0.4
C_f
0
0.1
0.2
0.3
0.4
0.5
0.6
C
$M = 1.0$
$M = 1.2$
$M = 1.4$
$M = 1.6$

(b)

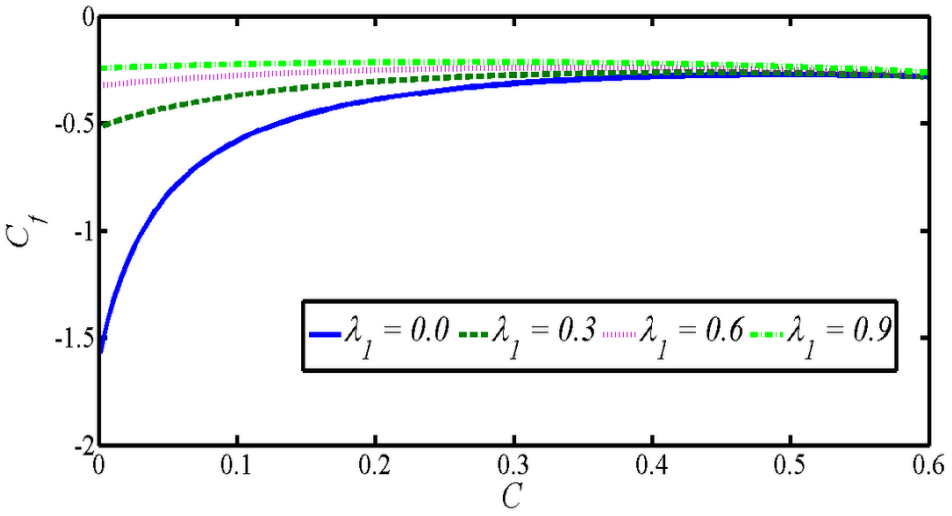

(c)

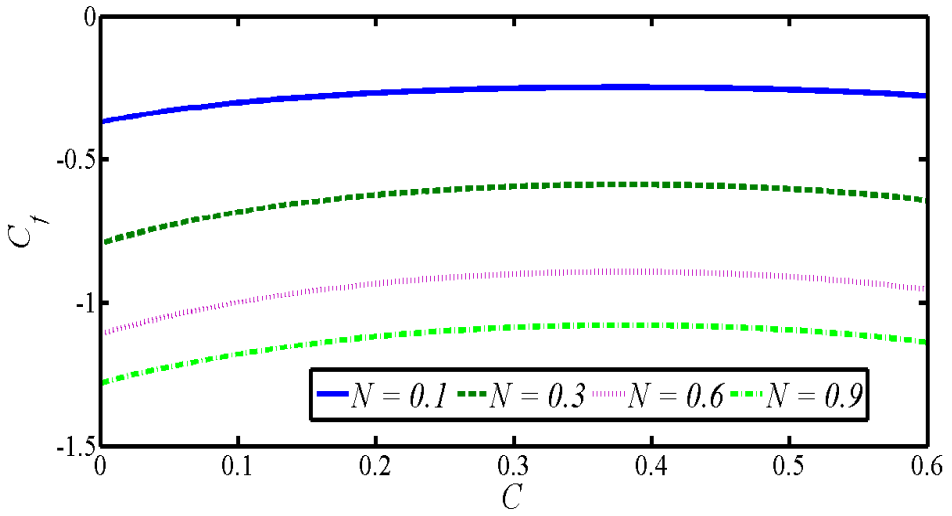

(d)

Figure 6: Effects of different fluid parameters on the skin friction profile for $(a)\ a = 0.5, b = 0.6, d = 1, x = 1, M = 1, \phi = \pi/3, Q = 2, \lambda_1 = 0.5, N = 0.1, m = 0.5, (b)\ a = 0.5, b = 0.6, d = 1, x = 1, \beta = 0.2, \phi = \pi/3, Q = 2, \lambda_1 = 0.5, N = 0.1, m = 0.5, (c)\ a = 0.5, b = 0.6, d = 1, x = 1, M = 1, \beta = 0.2, \phi = \pi/3, Q = 2, N = 0.1, m = 0.5, (d)\ a = 0.5, b = 0.6, d = 1, x = 1, M = 1, \beta = 0.2, \phi = \pi/3, Q = 2, \lambda_1 = 0.5, m = 0.5,$

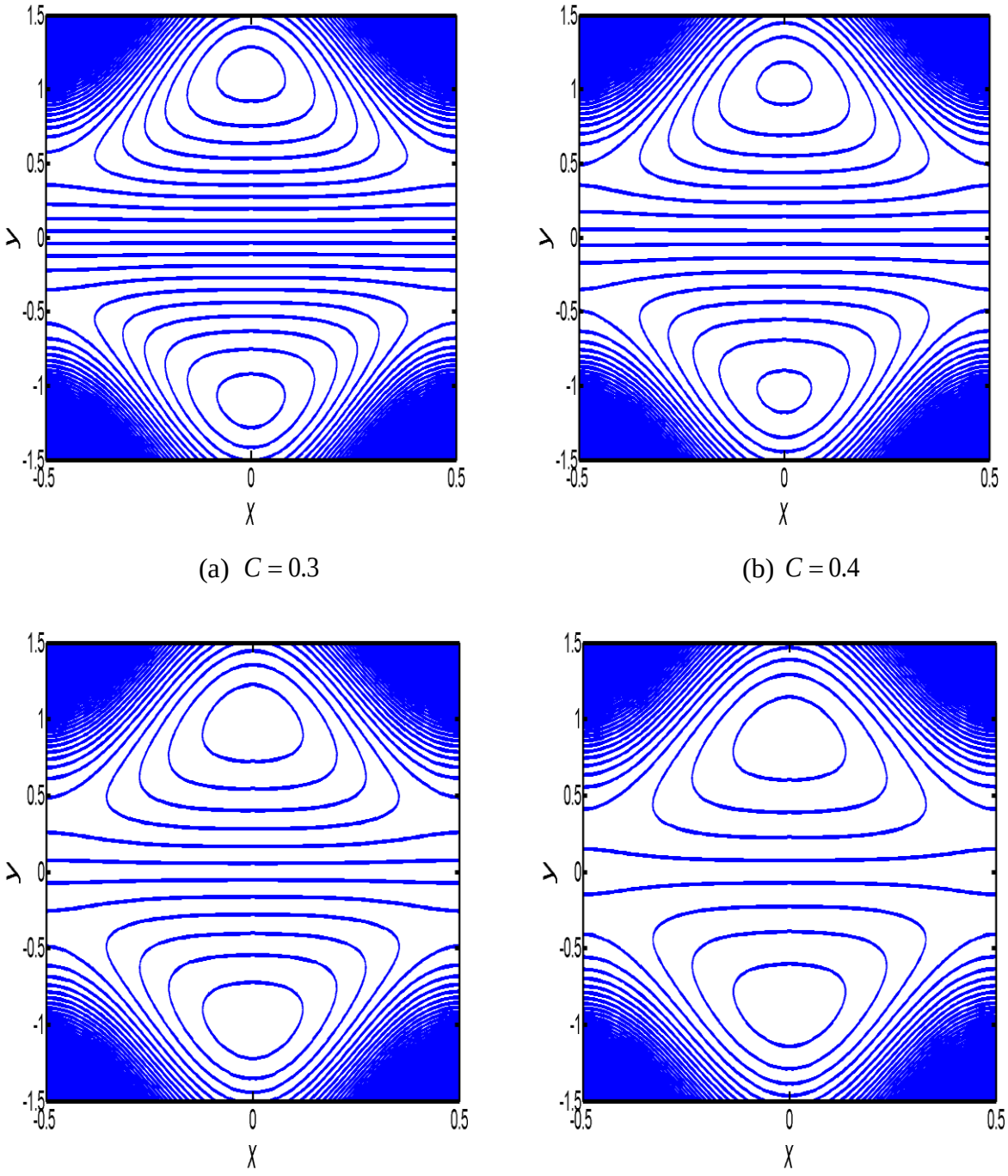

(a) $C = 0.3$ (b) $C = 0.4$

(c) $C = 0.5$ (d) $C = 0.6$

Figure 7: Streamline patterns for different values of volume fraction density of the particles for $a = 0.5, b = 0.5, d = 1, M = 1, \phi = 0, Q = 2, \lambda_1 = 0.5, N = 2, m = 0.5, \beta = 0.5.$

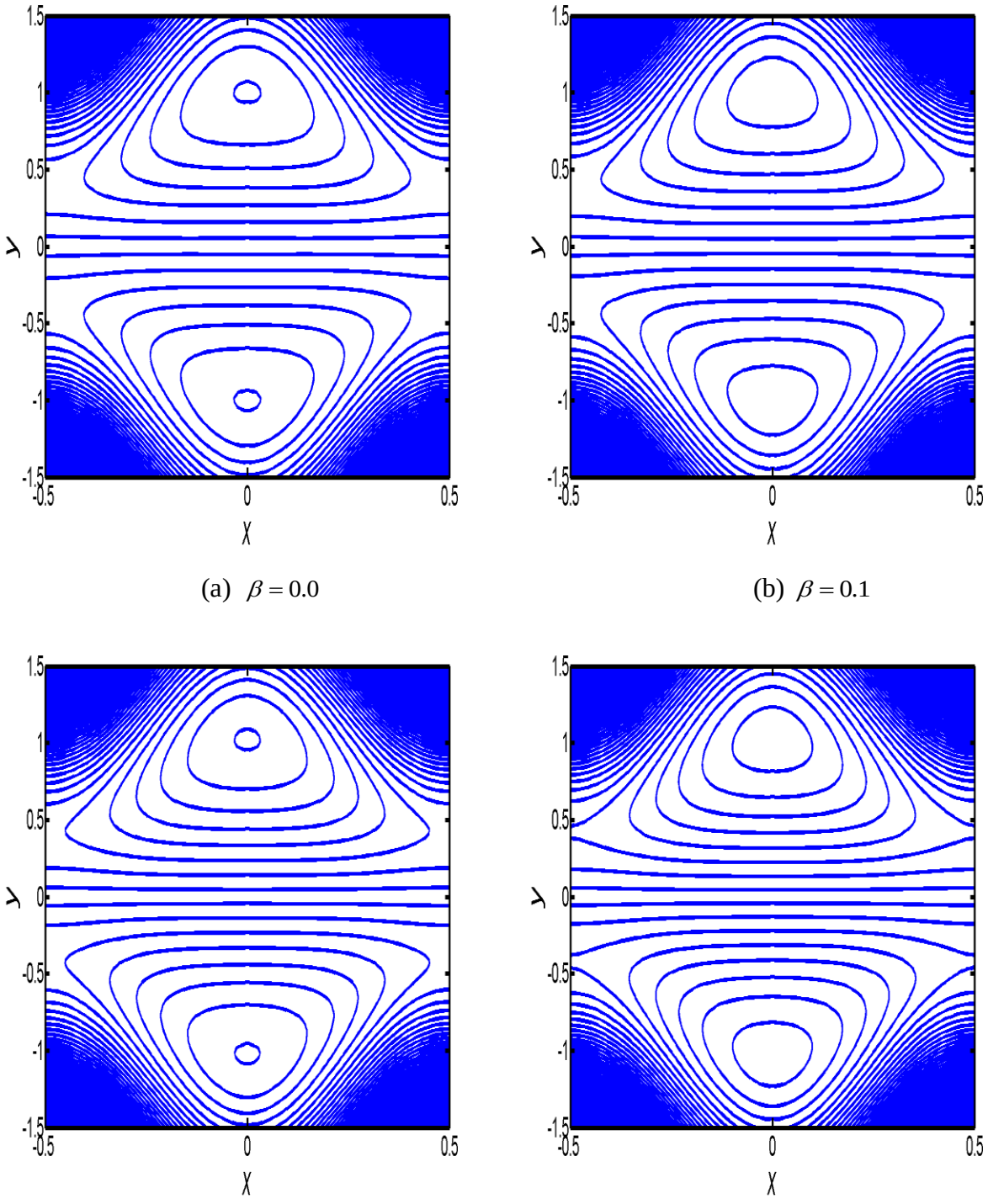

(a) $\beta = 0.0$ (b) $\beta = 0.1$

(c) $\beta = 0.2$ (d) $\beta = 0.5$

Figure 8: Streamline patterns for different values of slip parameter for $a = 0.5, b = 0.5, d = 1, M = 1, \phi = 0, Q = 2, \lambda_1 = 0.5, N = 1, m = 0.5, C = 0.4.$

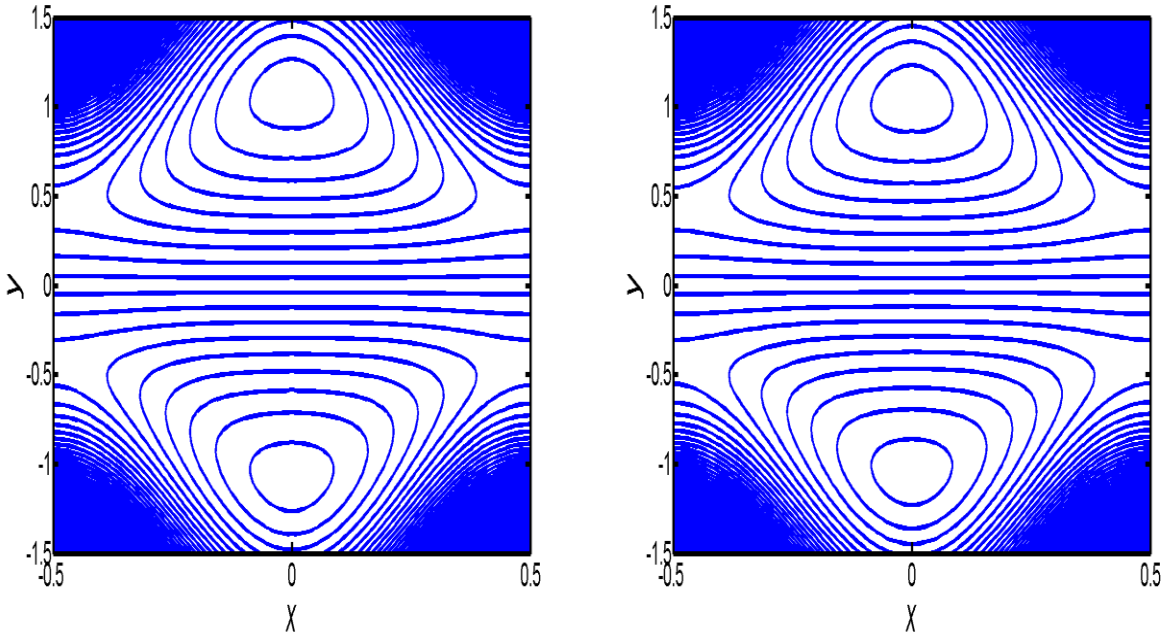

(a) $m = 0.0$ (b) $m = 0.5$

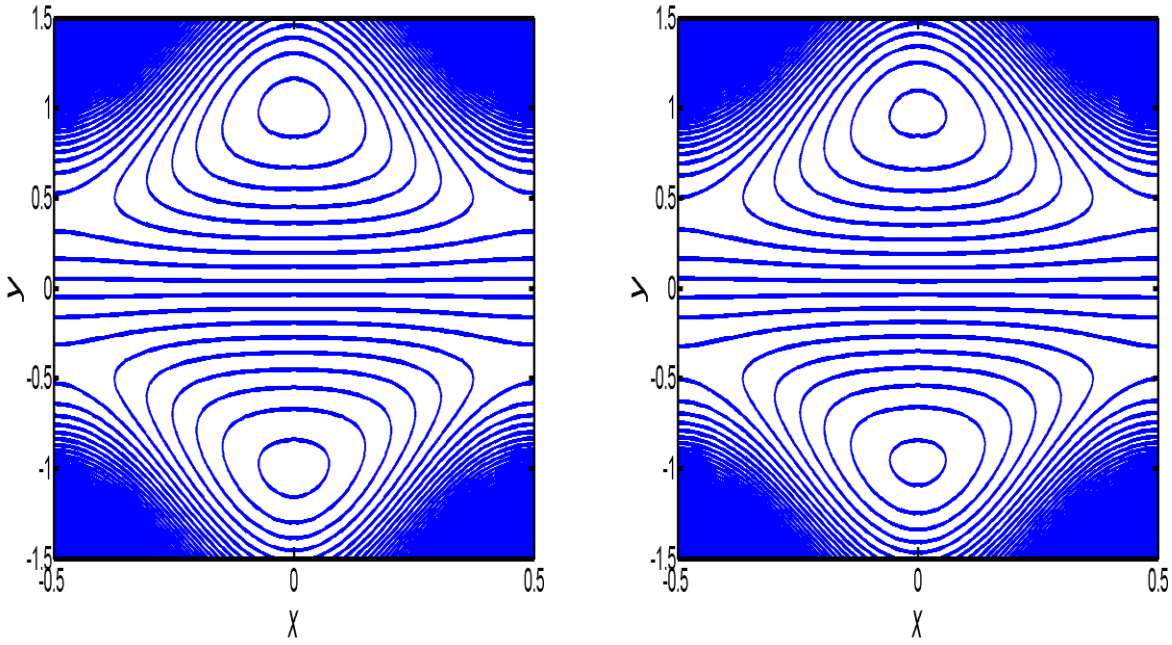

(c) $m = 1.0$ (d) $m = 1.5$

Figure 9: Streamline patterns for different values of Hall parameter for $a = 0.5, b = 0.5, d = 1, M = 1, \phi = 0, Q = 2, \lambda_1 = 0.5, N = 1, \beta = 0.5, C = 0.4.$

Figs. 2 a-f illustrate the impact of the Hall parameter (m), slip parameter (β), Hartmann magnetic number (M), viscoelastic parameter (λ_1), particulate suspension parameter (N) and volume fraction (C) on fluid phase velocity (u_f) distributions. In Fig. 2a an increase in the Hall current parameter clearly enhances the axial fluid velocity component across the micropump channel span. The parameter m arises as a quotient in the magnetic body force term, viz $-\frac{M^2}{1+m^2}\left(u_f+1\right)$ in the fluid phase momentum eqn. (24a). The presence of stronger Hall currents depletes the effect of the magnetic body force. This serves to accelerate the axial flow. The maximum axial fluid velocity therefore arises when Hall current vanishes ($m\rightarrow 0$). Similar observations have been made by Sutton and Sherman [49], Datta and Jana [50] etc. Symmetry of axial fluid velocity profiles is not broken by the Hall current effect. Peak velocity is consistently computed at the channel centerline. No overlap in profiles is observed. With increasing wall slip parameter (β), as seen in Fig. 2b, there is a distinct acceleration in fluid velocity at the channel boundaries; however towards the core zone of the channel the flow is decelerated. The non-adherence of the biofluid to the channel (pump duct) walls is maximized at the walls. This effect is progressively reduced with distance from the wall. The wall slip effect is therefore localized to the near-wall zones and is non-trivial here. Fig 2c shows that as magnetic Hartmann number is increased, there is a substantial retardation in the axial fluid phase velocity. The profiles also evolve from the classical parabolic configuration to strong oblate plateaus which are characteristic of MHD duct flows [50]. Maximum deceleration of the flow arises at the channel boundaries. Hartmann number effectively expresses the ratio of the Lorentz drag force to the hydrodynamic viscous force. The two forces are of the same order of magnitude when $M = 1$ and the former exceeds the latter for $M > 1$.Effective regulation (damping) of the axial flow is clearly attained with stronger magnetic fields i.e. higher Hartmann numbers. With increasing viscoelastic parameter (λ_1), as plotted in Fig. 2d, the relaxation time of the biofluid is increased relative to the retardation time. For small values of λ_1, the time scale of fluid movement is much greater than the relaxation time of elastic forces and behavior is closer to a normal viscous fluid. This manifests in acceleration in the flow. As values of λ_1, the elastic effect is greater and the fluid takes longer to respond to shear. This results in a strong deceleration in the flow. Again irrespective of non-Newtonian effect the symmetry in profiles is sustained across the micro-pump duct. Jefferys model is a special viscoelastic model which exhibits shear thinning characteristics, yield stress, and high shear viscosity. The Jeffreys

fluid model is known to degenerate to a Newtonian fluid at a very high wall shear stress, i.e., when wall stress is much greater than yield stress. It does however capture important characteristics of blood flow and deviates significantly from Newtonian results. With an increase in the particle drag suspension parameter, N, (Fig. 2e) there is a considerable reduction in axial fluid phase velocity. The presence of *larger particles* increases the drag coefficient in the flow. This induces flow retardation. For $N = 0$ the particle drag effect is negated and this is the case for single phase blood. Evidently the axial velocity is a maximum for this indicating that single phase models over-estimate values. At high N values a significant oblateness is generated in the profile which is absent for very small N values. Similar findings have been reported by for example Srivastava and Srivastava [38] and Kamel*et al.*[44]. Fig. 2f shows that with increasing volume fraction density of the particles (C), there is again a strong deceleration in the fluid phase velocity. This parameter is more related to the concentration of particles rather than their geometrical size. Interestingly the profiles, while modified, do not deviate from the parabolic case even at high values of C. Furthermore in all plots it is apparent that negative values of fluid phase velocity arise across the entire channel.

Figs. 3 a-f illustrate the response in particle phase velocity (u_p) distributions with a variation in respectively, the Hall parameter (m), slip parameter (β), Hartmann magnetic number (M), viscoelastic parameter (λ_1), particulate suspension parameter (N) and volume fraction (C). Comparing with figs. 2a-f, some similar trends are observed as with the fluid phase velocity. However two immediate differences are evident. Magnitudes of the particle phase velocity are an order of magnitude larger than fluid phase velocity and they are always positive indicating that the direction of motion is opposite. Of the six parameters studied all except the slip parameter arise in the fluid phase momentum conservation eqn. (24a). However only the suspension (drag) parameter, N, arises in the particle phase momentum conservation eqn. (24b). However both the slip parameter (β) and viscoelastic parameter (λ_1) feature in the fluid phase wall boundary conditions (25) and (26). The influence of Hall parameter (m), Hartmann magnetic number (M), viscoelastic parameter (λ_1), slip parameter (β) and volume fraction (C) on particle phase velocity is therefore experienced indirectly via coupling with the fluid phase momentum eqn. (24b). A much weaker decrement in particle phase velocity is witnessed over the same increment of Hall parameter (m) as shown in Fig. 3a. The parabolic characteristic profiles are retained however. With

greater wall slip effect (Fig. 3b), a much stronger enhancement in particle phase velocity at the walls is induced (magnitudes are approximately doubled) and the reduction zone in the core region is widened compared with the fluid velocity phase response (Fig. 2b). The depletion of particle velocity is also therefore generated in the core region as with the fluid phase velocity with greater wall hydrodynamic slip. Increasing Hartmann number, corresponding to stronger transverse magnetic field is found to cause the opposite response in particle phase velocity i.e. a marked elevation. The reduction in fluid phase momentum (Fig. 2c) is re-distributed to the suspended particles. This creates acceleration in particle phase velocity although the effect is less prominent than the fluid phase deceleration. The response to viscoelastic effect (Fig. 3d) is also very different compared with the fluid phase. Increasing relaxation to retardation time ratio is known to increase the orientation of rheological fluids in one direction and in polymers corresponds to enhancement in stretching. The blood therefore takes longer to relax in comparison with the rate at which the flow is deforming it as (λ_1) is enhanced. This is accompanied by stretching of the blood and increased delay in its return to the unstressed state. Fluid momentum development is therefore impeded and this is transferred to the suspended particles manifesting in acceleration. For the Newtonian case (λ_1=0) this effect is negated and the particle phase velocity is suppressed taking an approximately invariant profile across the micro-pump duct. The profiles evolve into parabolic plots across the micro-pump duct span with increasing viscoelastic effect. Fig. 3e indicates that increasing drag suspension parameter (N) results in a strong deceleration in the particle phase velocity, again the converse response to the fluid phase velocity (Fig. 2e). The enhanced drag effect (related to size of the suspended particles) will inevitably slow them down and simultaneously will enable acceleration of the fluid phase in the micro-pump duct. Although there is also a decrease in particle phase velocity with increasing volume fraction, C, as plotted in Fig. 3f, the impact is considerably more dramatic. Decreases from 20 for C = 0.05 to 4 for C = 0.20 at the duct centerline constituting a 500% decrease compared with a less than 10% depression for the fluid phase velocity over the same change in volume fraction. Concentration of suspended particles is massively elevated with increasing C values. This decreases the momentum distribution per particle considerably and results in substantial deceleration. The implication is therefore that dense blood suspensions will respond very differently to lighter suspensions in practical MHD pumping operations.

Figs. 4a-f depict the axial pressure gradient (*dp/dx*) response with axial coordinate (*x*) again for the six key control parameters i.e. Hartmann magnetic number (*M*), slip parameter (β), Hall parameter (*m*), viscoelastic parameter (λ_1), particulate suspension parameter (*N*) and volume fraction (*C*). Pressure gradient is significantly reduced with increasing Hartmann number i.e. less pressure per unit length is generated along the micro-pump duct. The periodic nature of the pressure gradient is captured in the snapshot given in Fig. 4a. Increasing slip is also found to strongly reduce the pressure gradient (Fig. 4b). This behavior is maintained along the duct length. The maximum pressure gradient corresponds to the no-slip case (β = 0). On the other hand an increase in Hall parameter demonstrably elevates the axial pressure gradient (Fig. 4c).The case of vanishing Hall parameter implies an absence of secondary (cross) flow in the duct. This achieves the lowest pressure gradient. The Hall current effect is therefore beneficial to pressure gradient enhancement. Increasing viscoelastic parameter (larger stress relaxation time of the blood), as illustrated in Fig. 4d, however impedes pressure gradient very strongly since it is associated with deceleration in the fluid phase. The Newtonian case (λ_1 =0) achieves the greatest axial pressure gradient which is consistent with other studies- see for example Shahidian *et al.* [49]. With increasing particle suspension (Fig. 4e) and volume fraction (Fig. 4f) pressure gradient is respectively increased and decreased considerably. In all the figures, positive values are sustained for *dp/dx* at all values of x i.e. reverse pressure gradient is not generated which is characteristic of peristaltic pumping and very attractive from the view point of more efficient MHD micro-pumps in medical applications. The magnetic field decelerates the peristaltic flow and therefore dramatically alters pressure distributions (velocity and pressure are inversely related). Slip also exerts an influence on velocity and momentum and this manifests in a modification in the pressure.

Figs. 5a-f present the pressure rise i.e. pressure difference across one wavelength (Δp_λ) with volumetric flow rate (*Q*) for again for the six key control parameters i.e. Hartmann magnetic number (*M*), slip parameter (β), Hall parameter (*m*), viscoelastic parameter (λ_1), particulate suspension parameter (*N*) and volume fraction (*C*). An advantage of peristaltic micro-pumps is that different pumping regimes can be achieved. These were first identified by Shapiro *et al.*[51] and designated as the *pumping region* ($\Delta p_\lambda > 0$), the *augmented pumping region* ($\Delta p_\lambda < 0$), and the *free pumping region* ($\Delta p_\lambda = 0$). Different responses are computed for the same parameter in these different regions Fig. 5a shows that in the *pumping region*, pressure difference slightly decreases

with increasing Hartmann number (*M*) whereas in the *augmented pumping region* it is enhanced. The transverse magnetic field therefore exerts a different influence depending on the pumping zone considered. In Fig. 5a and all other plots the Δp-Q relationship is clearly an *inverse linear relationship* i.e. pressure difference decreases with increasing volumetric flow rate which is also characteristic of peristaltic propulsion systems [52]. Fig 5b shows that with increasing wall slip the in the *pumping region*, pressure difference is also weakly reduced whereas in the *augmented pumping region* it is greatly elevated. Conversely with increasing Hall current parameter (m) as seen in fig 5c pressure difference is reduced in the augmented pumping zone whereas it is weakly increased in the pumping zone. Increasing viscoelastic parameter (Fig. 5d) strongly boosts the pressure difference in the augmented zone whereas it slightly reduces it in the pumping zone. Increasing drag suspension parameter, *N*, (Fig. 5e) significantly decreases pressure difference in the augmented region and causes an increase in the pumping region. A rise in volume fraction, *C*, (fig 5f) leads to a considerable boost in pressure difference in the augmented pumping zone and to a minute reduction in the pumping region. In all cases the maximum pressure difference is computed at the largest value of negative flow rate whereas the minimal pressure difference is obtained at the maximum positive flow rate.

Figs 6a-d depict the response in wall skin friction (dimensionless surface shear stress) with four selected control parameters, namely slip parameter (β), Hartmann magnetic number (*M*), viscoelastic parameter (λ_1) and particulate suspension parameter (*N*), plotted for variation in volume fraction (*C*). The skin friction is computed of course from the fluid phase velocity and is always negative. Increasing slip (Fig. 6a) is observed to generally enhance the skin friction, which is expected owing to the acceleration at the boundary with greater hydrodynamic slip, as computed earlier. Initially skin friction grows strongly with increasing particulate volume fraction. However a critical *C* values is reached beyond which the skin friction begins to decrease. This implies that an optimum concentration of suspended particles in the flowing blood exists up to which flow acceleration is attainable and above which it is lost. The peak skin friction corresponds to approximately $C = 0.35$. Fig 6b indicates that with increasing Hartmann number (*M*), skin friction is also enhanced and attains an optimal value between $C = 0.3$ and 0.4. The optimal value corresponds to a lower volume fraction progressively as Hartmann number is is increased i.e. the peak of the plot is displaced towards the left. With greater viscoelastic parameter the skin friction

is also elevated. The viscoelastic cases (λ_1>0) however achieve a much lower magnitude of skin friction at vanishing volume fraction (single phase streaming blood, C = 0) compared with the Newtonian case (λ_1=0). However unlike the response with variation in wall hydrodynamic slip parameter (β) and Hartmann number (M), the profiles in fig 6c converge as volume fraction reaches a peak value (0.6). The implication is that skin friction cannot grow indefinitely with greater viscoelasticity and will eventually attain a peak irrespective of the nature of the blood. Fig 6d demonstrates that with drag suspension parameter increasing (N) there is a sizeable reduction in skin friction which is physically viable. Again an optimum skin friction is attained at values of volume fraction, C, between 0.3 and 0.4. No asymptotic limit is attained for maximum volume fraction as in the case of the viscoelasticity variation (Fig. 6c).

Figs. 7a-d to 9a-d visualize the streamline distributions in the peristaltic flow regime volume fraction (C), slip parameter (β) and Hall current parameter (m), respectively. The entire micro-pump channel space is considered. These figures highlight a key characteristic of peristaltic flows, namely *trapping phenomena* which relate to the stream lines circulation and formation of a trapped bolus. Trapping permits the determination of reflux characteristics and also vortex growth and circulation intensity in peristaltic flows. Two sets of trapping zones are present – one above the centre line and one below and the structure is asymmetric owing to the imposition of different peristaltic waves at the lower and upper boundaries. These zones contain large boluses near the upper channel and lower channel with streamlines around the channel central zone remaining largely parallel and undistorted. In figs. 7a-d increasing volume fraction density of the particulate suspension is observed to encourage bolus growth in the upper and lower layers and eliminates the initially tightly constrained streamlines around the channel centerline. Volume fraction (C) features in the fluid phase momentum equation in the velocity difference term $\frac{NC}{(1-C)}\left(u_{p} - u_{f}\right)$. With increasing C values (with magnitudes which are always less than unity i.e. 0.3, 0.4, 0.5, 0.6 respectively in figs. 7a, b, c,d), for constant suspension parameter, N (=2), the fraction $C/(1-C)$ increases substantially from 3/7, to 2/3, 1 and to a maximum of 1.5. In the momentum eqn. (24a) the axial pressure gradient as defined below is positively influenced by the volume fraction term, $\frac{dp}{dx} = \frac{1}{1+\lambda_1}\frac{\partial^2 u_f}{\partial y^2} - \frac{M^2}{1+m^2}\left(u_f + 1\right) + \frac{NC}{\left(1-C\right)}\left(u_p - u_f\right)$, where it arises in the ultimate

term. This is characteristic of particulate flows i.e. suspensions. The increase in pressure gradient encourages a lateral spread in the trapped zones and this explains why enhancement in volume fraction density of the particulate suspension promotes bolus growth in the upper and lower layers and relaxes the streamline distributions around the central core zone. The impact of particle volume fraction increasing is to decelerate axial velocity and enhance pressure gradient, and this has also been observed by other researchers e.g. Bhatti and Zeeshan [67] and with extensive verification in terms of peristaltic pumping by Jiménez-Lozano *et al.* [68]. In figs 8a-d increasing slip parameter is also found to assist in bolus expansion in both upper and lower zones, although the central core streamlines are not modified to any great degree. Conversely in figs 9a-d with increase Hall current parameter there is a slight contraction in boluses and a weak intensification in streamlines near the channel centre axis.

5. CONCLUSIONS

A two-dimensional mathematical model has been developed to simulate the viscoelastic two-phase dynamics of blood in a peristaltic magnetohydrodynamic micro-pump with wall slip and Hall current effects. Stress relaxation and retardation in the blood have been studied via the Jefferys non-Newtonian model. The case of a two-dimensional asymmetric channel with different peristaltic wave trains propagating along the walls has been addressed. The transformed conservation equations for the fluid and particulate phases, with an appropriate particle drag factor incorporated have been solved analytically. Numerical evaluation of these solutions has been achieved. The computations have shown that:

- An increase in Hall current parameter decreases bolus growth in the channel, particle phase velocity and pressure difference in the augmented pumping region whereas it increases fluid phase velocity, axial pressure gradient and pressure difference in the pumping region.
- An increase in hydrodynamic slip parameter accelerates both particulate and fluid phase flow at and close to the channel walls, enhances wall skin friction, boosts pressure difference in the augmented pumping region and increases bolus magnitudes. However increasing wall slip decreases both particulate and fluid phase flow in the central (core) region, reduces pressure difference in the pumping region and strongly depresses axial pressure gradient across the channel span.
- Increasing Hartmann (magnetic) number decreases fluid phase velocity, enhances particle

phase velocity, decreases axial pressure gradient, elevates pressure difference in the augmented pumping region and decreases pressure difference in the pumping region.

- Increasing viscoelastic parameter (stress relaxation time to retardation time ratio) decelerates the fluid phase flow, accelerates the particle phase flow, decreases axial pressure gradient, elevates pressure difference in the augmented pumping region and reduces pressure difference in the pumping region.
- Increasing drag particulate suspension parameter decelerates the particle phase velocity, accelerates the fluid phase velocity, strongly elevates axial pressure gradient, reduces pressure difference (across one wavelength) in the augmented pumping region, weakly increases pressure difference in the classical pumping region and increases skin friction.
- Increasing particulate volume fraction density enhances bolus magnitudes in both the upper and lower zones of the channel and elevates pressure rise in the augmented pumping region whereas it decreases fluid phase velocity, particulate phase velocity, axial pressure gradient and weakly reduces pressure rise in the pumping region.

The current study has examined a relatively simple geometry for the MHD pumping duct (channel) and considered the biofluid (blood) to be two-phase and viscoelastic. Interesting characteristics have been computed of relevance to biomimetic magnetic micro-pumps. However, the geometry in real systems exhibits *curvature* and flows are also generically *three-dimensional* in nature. The careful analysis of these systems for better visualization of flow structures requires computational fluid dynamics (**CFD**) codes e.g. **ANSYS FLUENT, COMSOL Multiphysics, ADINA** etc. These allow the coupled solution for Maxwell electromagnetic fields with multi-phase material models and laminar/turbulent flows and also deformable conduits (fluid structure interaction) are currently being explored [10]. Furthermore, more generalized viscoelastic models in conjunction with Eringen micro-morphic models (which simulate spin of particles in blood suspensions) will undoubtedly provide a deeper insight into the biorheology of such pumping systems and this aspect is also being considered [69, 70].

REFERENCES

[1] L. Pauling, C.D. Coryell, The magnetic properties and structure of hemoglobin, oxyhemoglobin and carbonmonoxyhemoglobin, Proceedings of the National Academy of Sciences, 22 (1936) 210-216.

[2] M. Motta, Y. Haik, A. Gandhari, C.-J. Chen, High magnetic field effects on human deoxygenated hemoglobin light absorption, Bioelectrochemistry and bioenergetics, 47 (1998) 297-300.

[3] V. Mooney, A randomized double-blind prospective study of the efficacy of pulsed electromagnetic fields for interbody lumbar fusions, Spine, 15 (1990) 708-712.

[4] W. Sharrard, A double-blind trial of pulsed electromagnetic fields for delayed union of tibial fractures, Journal of Bone & Joint Surgery, 72 (1990) 347-355.

[5] C.T. Rubin, K.J. McLeod, L.E. Lanyon, Prevention of osteoporosis by pulsed electromagnetic fields, Journal of Bone & Joint Surgery, 71 (1989) 411-417.

[6] D. Wyatt, The electromagnetic blood flowmeter, Journal of Physics E: Scientific Instruments, 1 (1968) 1146.

[7] K. Qian, P. Zeng, W. Ru, H. Yuan, New concepts and new design of permanent maglev rotary artificial heart blood pumps, Medical engineering & physics, 28 (2006) 383-388.

[8] E.A. Dehkordi, M.E. Moghadam, M.B. Shafii, A Novel Hydro Magnetic Micro-Pump and Flow Controller, in: ASME 2008 6th International Conference on Nanochannels, Microchannels, and Minichannels, American Society of Mechanical Engineers, (2008) 1537-1544.

[9] S. Naceur, F.Z. Kadid, R. Abdessemed, The study of the electroconductive liquids flow in a conduction magnetohydrodynamic pump, Transactions on Electrical and Electronic Materials, 17 (2016) 252-256.

[10] M.I. Hasan, A.J.F. Ali, R.S. Tufah, Numerical study of the effect of channel geometry on the performance of magnetohydrodynamic micro pump, Engineering Science and Technology, an International Journal, 20 (2017) 982-989.

[11] A. Homsy, S. Koster, J.C. Eijkel, A. Van Den Berg, F. Lucklum, E. Verpoorte, N.F. De Rooij, A high current density DC magnetohydrodynamic (MHD) micropump, Lab on a Chip, 5 (2005) 466-471.

[12] V. Patel, S.K. Kassegne, Electroosmosis and thermal effects in magnetohydrodynamic (MHD) micropumps using 3D MHD equations, Sensors and Actuators B: Chemical, 122 (2007) 42-52.

[13] G. Zhao, Y. Jian, L. Chang, M. Buren, Magnetohydrodynamic flow of generalized Maxwell fluids in a rectangular micropump under an AC electric field, Journal of Magnetism and Magnetic Materials, 387 (2015) 111-117.

[14] S. Pal, A. Datta, S. Sen, A. Mukhopdhyay, K. Bandopadhyay, R. Ganguly, Characterization of a ferrofluid-based thermomagnetic pump for microfluidic applications, Journal of Magnetism and Magnetic Materials, 323 (2011) 2701-2709.

[15] H.S. Kabbani, M.J. Mack, S.W. Joo, S. Qian, Analytical prediction of flow field in magnetohydrodynamic-based microfluidic devices, Journal of Fluids Engineering, 130 (2008) 091204.

[16] Y. Jian, D. Si, L. Chang, Q. Liu, Transient rotating electromagnetohydrodynamic micropumps between two infinite microparallel plates, Chemical Engineering Science, 134 (2015) 12-22.

[17] S. Rashidi, J.A. Esfahani, M. Maskaniyan, Applications of magnetohydrodynamics in biological systems-a review on the numerical studies, Journal of Magnetism and Magnetic Materials, 439 (2017) 358-372.

[18] F.L. Sinatra, Understanding the interaction between blood flow and an applied magnetic field, (2010). *Graduate Theses and Dissertation.*

[19] O.A. Bég, L. Sim, J. Zueco, R. Bhargava, Numerical study of magnetohydrodynamic viscous plasma flow in rotating porous media with Hall currents and inclined magnetic field influence, Communications in Nonlinear Science and Numerical Simulation, 15 (2010) 345-359.

[20] A.V. Lemoff, A.P. Lee, An AC magnetohydrodynamic micropump, Sensors and Actuators B: Chemical, 63 (2000) 178-185.

[21] D. Srnivasacharya, M. Shiferaw, MHD flow of micropolar fluid in a rectangular duct with hall and ion slip effects, Journal of the Brazilian Society of Mechanical Sciences and Engineering, 30 (2008) 313-318.

[22] J.P. Montoya, S.I. Merz, R.H. Bartlett, Laboratory experience with a novel, non-occlusive, pressure-regulated peristaltic blood pump, ASAIO journal (American Society for Artificial Internal Organs: 1992), 38 (1991) M406-411.

[23] S. Natarajan, M. Mokhtarzadeh-Dehghan, Numerical prediction of flow in a model of a (potential) soft acting peristaltic blood pump, International journal for numerical methods in fluids, 32 (2000) 711-724.

[24] C. Jaggy, M. Lachat, B. Leskosek, G. Zünd, M. Turina, Affinity pump system: a new peristaltic blood pump for cardiopulmonary bypass, Perfusion, 15 (2000) 77-83.

[25] T. Pan, E. Kai, M. Stay, V. Barocas, B. Ziaie, A magnetically driven PDMS peristaltic micropump, in: Engineering in Medicine and Biology Society, 2004. IEMBS'04. 26th Annual International Conference of the IEEE, IEEE, 2004, pp. 2639-2642.

[26] D. Tripathi, O.A. Bég, A study of unsteady physiological magneto-fluid flow and heat transfer through a finite length channel by peristaltic pumping, Proceedings of the institution of mechanical Engineers, Part H: Journal of Engineering in Medicine, 226 (2012) 631-644.

[27] M. Kothandapani, S. Srinivas, On the influence of wall properties in the MHD peristaltic transport with heat transfer and porous medium, Physics Letters A, 372 (2008) 4586-4591.

[28] K.S. Mekheimer, Peristaltic flow of blood under effect of a magnetic field in a non-uniform channels, Applied Mathematics and Computation, 153 (2004) 763-777.

[29] M.M. Bhatti, A. Zeeshan, R. Ellahi, Simultaneous effects of coagulation and variable magnetic field on peristaltically induced motion of Jeffrey nanofluid containing gyrotactic microorganism, Microvascular Research, 110 (2017) 32-42.

[30] N. Ijaz, A. Zeeshan, M.M. Bhatti, R. Ellahi, Analytical study on liquid-solid particles interaction in the presence of heat and mass transfer through a wavy channel, Journal of Molecular Liquids, 250 (2018) 80-87.

[31] M.M. Bhatti, M. Sheikholeslami, A. Zeeshan, Entropy analysis on electro-kinetically modulated peristaltic propulsion of magnetized nanofluid flow through a microchannel. *Entropy 19 (*2017) 481.

[32] M.M. Bhatti, A. Zeeshan, R. Ellahi, Heat transfer with thermal radiation on MHD particle–fluid suspension induced by metachronal wave, Pramana, 89 (2017) 48.

[33] A. Zeeshan, N. Ijaz, M.M. Bhatti, A.B. Mann, Mathematical study of peristaltic propulsion of solid–liquid multiphase flow with a biorheological fluid as the base fluid in a duct, Chinese Journal of Physics, 55(4) (2017) 1596-1604.

[34] D. Tripathi, O.A. Bég, J.L. Curiel-Sosa, Homotopy semi-numerical simulation of peristaltic flow of generalised Oldroyd-B fluids with slip effects, Computer methods in biomechanics and biomedical engineering, 17 (2014) 433-442.

[35] M.J. Uddin, M. Kabir, O.A. Bég, Computational investigation of Stefan blowing and multiple-slip effects on buoyancy-driven bioconvection nanofluid flow with microorganisms, International Journal of Heat and Mass Transfer, 95 (2016) 116-130.

[36] M. Rivero, S. Cuevas, Analysis of the slip condition in magnetohydrodynamic (MHD) micropumps, Sensors and actuators B: Chemical, 166 (2012) 884-892.

[37]O.A. Bég, M.F. Basir, M. Uddin, A.M. Ismail, Numerical study of slip effectson unsteady aysmmetric bioconvective nanofluid flow in a porous microchannel with anexpanding/ contracting upper wall using Buongiorno's model, Journal of Mechanics in Medicine and Biology, 17 (2016) 1750059.

[38] O.A. Bég, J. Zueco, L. Lopez-Ochoa, Network numerical analysis of optically thick hydromagnetic slip flow from a porous spinning disk with radiation flux, variable thermophysical properties, and surface injection effects, Chemical Engineering Communications, 198 (2010) 360-384.

[39] M.J. Uddin, W.A. Khan, A.I.M. Ismail, O.A. Bég, Computational study of three-dimensional stagnation point nanofluid bioconvection flow on a moving surface with anisotropic slip and thermal jump effect, Journal of Heat Transfer, 138 (2016) 104502-104502-104507.

[40] E. El-Shehawy, N. El-Dabe, I. El-Desoky, Slip effects on the peristaltic flow of a non-Newtonian Maxwellian fluid, Acta Mechanica, 186 (2006) 141-159.

[41] N. Ali, Q. Hussain, T. Hayat, S. Asghar, Slip effects on the peristaltic transport of MHD fluid with variable viscosity, Physics Letters A, 372 (2008) 1477-1489.

[42] S. Chien, Biophysical behavior of red cells in suspensions, The red blood cell, 2 (1975) 1031-1133.

[43] L. Srivastava, V. Srivastava, Peristaltic transport of a particle-fluid suspension, Journal of Biomechanical Engineering, 111 (1989) 157-165.

[44] T. Bég, M. Rashidi, O.A. Bég, N. Rahimzadeh, Differential transform semi-numerical analysis of biofluid-particle suspension flow and heat transfer in non-Darcian porous media, Computer methods in biomechanics and biomedical engineering, 16 (2013) 896-907.

[45] S. Chhabra, A.K. Prasad, Flow and particle dispersion in a pulmonary alveolus—Part II: Effect of gravity on particle transport, Journal of biomechanical engineering, 132 (2010) 051010.

[46] M. Bhatti, A. Zeeshan, N. Ijaz, O.A. Bég, A. Kadir, Mathematical modelling of nonlinear thermal radiation effects on EMHD peristaltic pumping of viscoelastic dusty fluid through a porous medium duct, Engineering science and technology, an international journal, 20 (2017) 1129-1139.

[47] V. Srivastava, L. Srivastava, Effects of Poiseuille flow on peristaltic transport of a particulate suspension, Zeitschrift für Angewandte Mathematik und Physik (ZAMP), 46 (1995) 655-679.

[48] A. Medhavi, U. Singh, A two-layered suspension flow induced by peristaltic waves, International Journal of Fluid Mechanics Research, 35 (2008).

[49] M.H. Kamel, I.M. Eldesoky, B.M. Maher, R.M. Abumandour, Slip effects on peristaltic transport of a particle-fluid suspension in a planar channel, Applied bionics and biomechanics, 2015 (2015).

[50] M. Bahiraei, Particle migration in nanofluids: A critical review, International Journal of Thermal Sciences, 109 (2016) 90-113

[51] M. Bahiraei, A comprehensive review on different numerical approaches for simulation in nanofluids: Traditional and novel techniques, Journal of Dispersion Science and Technology, 35(7) (2014) 984-996.

[52] M. Bahiraei, A numerical study of heat transfer characteristics of CuO–water nanofluid by Euler-Lagrange approach, Journal of Thermal Analysis and Calorimetry, 123(2) (2016) 1591-1599.

[53] M. Bahiraei, N. Mazaheri, M. Alighardashi, Development of chaotic advection in laminar flow of a non-Newtonian nanofluid: A novel application for efficient use of energy, Applied Thermal Engineering, 124 (2017) 1213-1223.

[54] M. Bahiraei, K. Gharagozloo, M. Alighardashi, N. Mazaheri, CFD simulation of irreversibilities for laminar flow of a power-law nanofluid within a minichannel with chaotic perturbations: An innovative energy-efficient approach, Energy Conversion and Management, 144 (2017) 374-387.

[55] M. Bahiraei, R. Khosravi, S. Heshmatian, Assessment and optimization of hydrothermal characteristics for a non-Newtonian nanofluid flow within miniaturized concentric-tube heat exchanger considering designer's viewpoint, Applied Thermal Engineering, 123 (2017) 266-276.

[56] A. Shahidian, M. Ghassemi, S. Khorasanizade, M. Abdollahzade, G. Ahmadi, Flow analysis of non-Newtonian blood in a magnetohydrodynamic pump, IEEE transactions on magnetics, 45 (2009) 2667-2670.

[57] R. Bird, Armstrong and RC Hassager, O.,"Dynamics of Polymeric Liquids". v. 1, in, John Wiley & Sons, USA, 1987.

[58] D. Gutierrez-Lemini, Engineering Viscoelasticity, Springer US, New York, 2014.

[59] S.E. Charm, G.S. Kurland, Blood flow and microcirculation, American Heart Journal, 88 (1974) 815.

[60] G.W. Sutton, A. Sherman, Engineering magnetohydrodynamics, McGraw-Hill, New York a.o, 1965.

[61] N. Datta, R.N. Jana, Hall effects on hydromagnetic convective flow through a channel with conducting walls, International Journal of Engineering Science, 15 (1977) 561-567.

[62] A.H. Shapiro, M.Y. Jaffrin, S.L. Weinberg, Peristaltic pumping with long wavelengths at low Reynolds number, Journal of Fluid Mechanics, 37 (1969) 799-825.

[63] Y. Fung, Biomechanical aspects of growth and tissue engineering, in: Biomechanics, Springer, 1990, pp. 499-546.

[64] T. Hayat, N. Aslam, M. Rafiq, F.E. Alsaadi, Hall and Joule heating effects on peristaltic flow of Powell-Eyring liquid in an inclined symmetric channel, Results in Physics, 7 (2017) 518-528.

[65] K.S. Mekheimer, Y. Abd elmaboud, Peristaltic transport of a particle-fluid suspension through a uniform and non-uniform annulus, Applied Bionics and Biomechanics, 5(2) 47-57.

[66] M.M. Bhatti, A. Zeeshan, R. Ellahi, Study of heat transfer with nonlinear thermal radiation on sinusoidal motion of magnetic solid particles in a dusty fluid, Journal of Theoretical and Applied Mechanics, 46(3) (2016) 75-94.

[67] M. M. Bhatti and A. Zeeshan, Heat and mass transfer analysis on peristaltic flow of particle–fluid suspension with slip effects, J. Mech. Med. Biol. **17**, 1750028 (2017) [16 pages]

[68] J. Jiménez-Lozano et al., Analysis of peristaltic two-phase flow with application to ureteral biomechanics, Acta Mechanica, 219, 91–109 (2011).

[69] Mohamed El Gendy, O. Anwar Bég, A. Kadir, M.N. Islam and D. Tripathi, ANSYS FLUENT Computational fluid dynamics simulation and visualization of Newtonian and non-Newtonian transport in a peristaltic micro-pump, J. Mechanics in Medicine and Biology (2018).***Under review***

[70] O. Anwar Bég, A. Kadir, M.N. Islam and Mohamed El Gendy, FSI two-way simulation of micropolar magnetohydrodynamic peristaltic pumping, J. Biomechanics (2018). ***Submitted***